

Determining parameters of Moon's orbital and rotational motion from LLR observations using GRAIL and IERS-recommended models

Dmitry A. Pavlov · James G. Williams ·
Vladimir V. Suvorkin

Received: 14 Jan 2016 / Accepted: 25 Jun 2016

The final publication is available at Springer via
<http://dx.doi.org/10.1007/s10569-016-9712-1>

Abstract The aim of this work is to combine the model of orbital and rotational motion of the Moon developed for DE430 with up-to-date astronomical, geodynamical, and geo- and selenophysical models. The parameters of the orbit and physical libration are determined in this work from lunar laser ranging (LLR) observations made at different observatories in 1970-2013. Parameters of other models are taken from solutions that were obtained independently from LLR.

A new implementation of the DE430 lunar model, including the liquid core equations, was done within the EPM ephemeris. The postfit residuals of LLR observations make evident that the terrestrial models and solutions recommended by the IERS Conventions are compatible with the lunar theory. That includes: EGM2008 gravitational potential with conventional corrections and variations from solid and ocean tides; displacement of stations due to solid and ocean loading tides; and precession-nutation model. Usage of these models in the solution for LLR observations has allowed us to reduce the number of parameters to be fit. The fixed model of tidal variations of the geopotential has resulted in a lesser value of Moon's extra eccentricity rate, as compared to the original DE430 model with two fit parameters.

A mixed model of lunar gravitational potential was used, with some coefficients determined from LLR observations, and other taken from the GL660b solution obtained from the GRAIL spacecraft mission.

Solutions obtain accurate positions for the ranging stations and the five retroreflectors. Station motion is derived for sites with long data spans. Dissipation is detected at the lunar fluid core-solid mantle boundary demonstrating that a fluid

D. A. Pavlov (✉), V. V. Suvorkin
Institute of Applied Astronomy RAS, Kutuzov embankment 10, St. Petersburg, 191187,
Russia
E-mail: dpavlov@iaaras.ru

J. G. Williams
Jet Propulsion Laboratory, California Institute of Technology, Pasadena, CA 91109, USA

core is present. Tidal dissipation is strong at both Earth and Moon. Consequently, the lunar semimajor axis is expanding by 38.20 mm/yr, the tidal acceleration in mean longitude is $-25.90''/\text{cy}^2$, and the eccentricity is increasing by 1.48×10^{-11} each year.

Keywords Lunar laser ranging · Lunar physical libration · Tidal variations of geopotential

1 Introduction

Lunar laser ranging (LLR) has been the most precise way to determine the orbit and physical libration of the Moon since 1970. Several groups across the world issue lunar ephemerides, most notably NASA JPL (Williams et al. 2001; Folkner et al. 2014), IAA RAS (Krasinsky 2002; Krasinsky et al. 2011; Vasilyev and Yagudina 2014), and IMCCE (Manche et al. 2008, 2012; Fienga et al. 2013). Equations of motion, algorithms of reductions of observations, and sets of determined parameters are not identical across groups, although they have much in common. A number of choices arise regarding parameters of gravitational potential of Earth and Moon: one can determine them from LLR, or use preset solutions obtained from gravimetry measurements. An additional choice is whether to determine parameters of Earth’s nutation from LLR or use a preset model with daily corrections obtained from VLBI observations.

In this work, preset solutions are explored in the context of their compatibility with lunar ranging observations:

- Conventional model of geopotential and its tidal variations;
- IAU 2000/2006 precession-nutation model with available EOP series;
- GL660b model of lunar gravitational potential;
- GNSS solutions for stations’ drift (for selected stations).

A completely new implementation compatible with the DE430 lunar integration model was done on top of the implementation of the EPM ephemerides (Pitjeva 2013; Pitjeva and Pitjev 2014), along with a new implementation of reduction of LLR observations. No original DE430 program code was used in this work. The Moon was integrated along with the whole Solar system; for the rest of the Solar system model, EPM’s dynamical equations were used.

2 Observations

Observations were processed from all stations that have their LLR data publicly available. Table 1 shows the number and timespan of observations processed from each station.

Apache Point observations were downloaded from the APOLLO website (http://physics.ucsd.edu/~tmurphy/apollo/norm_pts.html). Observations for the rest of the stations were downloaded from the Lunar Analysis Center of Paris Observatory (<http://polac.obspm.fr/llrdatae.html>). All the downloaded files are in so-called “MINI” format (one line per normal point).

Some uncertainties provided with the normal points were changed before determination of model parameters. Uncertainties of Apache Point observations were

Station	Timespan	# of normal points
McDonald, TX, USA	1970–1985	3604
MLRS1, TX, USA	1983–1988	631
MLRS2, TX, USA	1988–2013	3653
Haleakala, HI, USA	1984–1990	770
CERGA, France (Ruby laser)	1984–1986	1188
CERGA, France (YAG laser)	1987–2005	8324
CERGA, France (MeO laser)	2009–2013	654
Matera, Italy	2003–2013	83
Apache Point, NM, USA	2006–2012	1573
total	1970–2013	20480

Table 1 Lunar laser ranging observations available as normal points

scaled up as recommended on the APOLLO website. Provided normal points of Matera for the period of 4 December 2011 to 9 November 2012 have unrealistically small (few ps) uncertainties and have been fixed to 83.4 ps (2.5 cm). For other stations, selected groups of normal points were scaled up to match the postfit weighted root-mean-square (wrms). Scaling was done when the postfit wrms was higher than the rms of provided uncertainties by a 20% margin or more. The groups were formed following the big-picture behavior of the provided uncertainties. The reweighting is summarized in Table 2. After refitting of the reweighted observations, none of postfit wrms (see section 7.3) exceeds the rms of provided uncertainties by more than 20%.

Station	Timespan	factor	explanation
Haleakala	all	$\times 1.4$	provided 4.1 cm, postfit 5.8 cm
McDonald	all	$\times 1.2$	provided 16.8 cm, postfit 20.1 cm
MLRS1	before 06.09.1985	$\times 1.2$	provided 34.7 cm, postfit 41.7 cm
MLRS1	after 06.09.1985	$\times 2.3$	provided 2.8 cm, postfit 6.4 cm
MLRS2	before 18.06.1999	$\times 1.6$	provided 2.1 cm, postfit 3.5 cm
CERGA	30.10.1991–07.09.1992	$\times 1.8$	provided 3.1 cm, postfit 5.7 cm
CERGA	06.12.1993–01.01.1995	$\times 1.2$	provided 3.3 cm, postfit 4.0 cm
CERGA	01.01.1995–11.11.1998	$\times 1.9$	provided 1.6 cm, postfit 3.1 cm
Apache	04.04.2006–30.10.2010	$\times 2.0$	“group a” scaling by APOLLO
Apache	01.12.2010–06.04.2012	$\times 6.0$	“group b” scaling by APOLLO
Apache	07.04.2012–28.02.2012	$\times 2.5$	“group c” scaling by APOLLO
Matera	04.12.2011–09.11.2012	to 2.5 cm	too small provided uncertainties

Table 2 Reweighting of selected observations. Date notation is DD.MM.YYYY

More recent available observations were deliberately left out, in order to facilitate possible comparison of the obtained results with already published lunar ephemerides (Fienga et al. 2013; Folkner et al. 2014; Vasilyev and Yagudina 2014).

3 Dynamical model

3.1 Planetary part

The modeled motion of the Sun, the planets, and the Moon (as point-masses) obeys the Einstein-Infeld-Hoffmann relativistic equations in inertial barycentric frame and TDB timescale, with additional perturbations from:

- solar oblateness;
- 301 largest asteroids and 30 largest trans-Neptunian objects (TNO);
- a two-dimensional asteroid annulus;
- a one-dimensional TNO ring.

For details on planetary equations, we refer to (Pitjeva 2013; Pitjeva and Pitjev 2014) and (Folkner et al. 2014). The rest of this section describes the geocentric motion of the Moon and its rotation.

3.2 Orbit of the Moon

The following perturbations are included in the dynamical equations of the geocentric motion of the Moon:

- interaction between the Moon’s figure and bodies considered as point masses (Earth, Sun, Venus, Mars and Jupiter);
- interaction between Earth’s figure and bodies considered as point masses (Moon, Sun, Venus, Mars and Jupiter);
- interaction between the distorted part of the Earth (due to solid tides raised by the Moon and the Sun) and the Moon.

Acceleration of a point-mass m due to a body’s disturbed gravitational potential is calculated from the normalized spherical harmonic terms \bar{C}_{nm} and \bar{S}_{nm} :

$$\frac{\mathbf{f}_{\text{fig-pm}}}{m} = \mu \text{Re} \left[\sum_{n=2}^{n_{\text{max}}} R^n \sum_{m=0}^n (\bar{C}_{nm} - i\bar{S}_{nm}) \nabla \bar{V}_{nm}(r, \lambda, \phi) \right]$$

$$\bar{V}_{nm}(r, \lambda, \phi) = N_{nm} \frac{\cos m\lambda + i \sin m\lambda}{r^{n+1}} P_n^m(\sin \phi) \quad (1)$$

$$N_{nm} = \sqrt{\frac{(n-m)!(2n+1)!(2-\delta_{0m})}{(n+m)!}}$$

Where: μ is the body’s standard gravitational parameter; R is the body’s radius; r , λ , and ϕ are the distance, longitude, and latitude of the point-mass in the body’s frame; P_n^m is the associated Legendre function of degree n and order m . \bar{C}_{nm} and \bar{S}_{nm} are normalized spherical harmonic terms commonly found in published solutions; the unnormalized terms $C_{nm} = N_{nm}\bar{C}_{nm}$ and $S_{nm} = N_{nm}\bar{S}_{nm}$ were introduced in (Cunningham 1970). The resulting acceleration should be rotated from the body’s frame to inertial frame. We refer to (Krasinsky and Vasilyev 2006) for the recursive equations used to calculate $\nabla \bar{V}_{nm}(r, \lambda, \phi)$. n_{max} is a chosen limit of the degree of expansion of the body’s gravitational potential. In this work, n_{max} is 6 for both Earth and Moon. Effects from higher degrees has proven to be unnoticeably small at the present level of observations.

The Moon and the Sun raise periodical ocean and solid tides on the Earth (there is also an additional constant distortion of $C_{20,E}$ caused by the Sun and the Moon). Two approaches can be made to account for the perturbations of the orbital motion of the Moon due to these tides. Throughout this paper, we will reference to them as the ‘‘IERS tidal model’’ and the ‘‘DE tidal model’’.

3.2.1 IERS tidal model: variations of spherical harmonic coefficients

It is recommended by the IERS Conventions (Petit and Luzum 2010) that the changes induced by the solid and ocean tides are modeled as variations in the coefficients \bar{C}_{nm} and \bar{S}_{nm} . Only corrections up to order and degree 2 are taken. Solid tide corrections for ‘‘conventional tide free’’ EGM2008 are computed in two steps. At first the frequency-independent part is computed:

$$\Delta\bar{C}_{nm,E} - i\Delta\bar{S}_{nm,E} = \frac{k_{nm}}{2n+1} \sum_{j=M,S} \frac{\mu_j}{\mu_E} \left(\frac{R_E}{r_j}\right)^{n+1} \bar{P}_{nm}(\sin\Phi_j) e^{-im\lambda_j} \quad (2)$$

where μ_E , μ_M , and μ_S are the standard gravitational parameters of the Earth, Moon, and Sun respectively; $\bar{P}_{nm} = P_n^m N_{nm}$ is the normalized associated Legendre polynomial, and the Love numbers k_{nm} correspond to those (nm) coefficients being corrected. Since elastic properties of the Earth are frequency dependent, on the second step one should compute additional corrections from the respective bands to the coefficients using frequency dependent Love numbers different from respective nominal values. The correction for $\bar{C}_{20,E}$ from the long period components is:

$$\Delta\bar{C}_{20}^{(fd)} = \text{Re} \sum_f (A_0 \delta k_f H_f) e^{i\theta_f} \quad (3)$$

and the corrections to \bar{C}_{2m} and \bar{S}_{2m} from diurnals ($m = 1$) and semidiurnals ($m = 2$) are given by

$$\begin{cases} \Delta\bar{C}_{21}^{(fd)} - i\Delta\bar{S}_{21}^{(fd)} = -i \sum_f (A_1 \delta k_f H_f) e^{i\theta_f} \\ \Delta\bar{C}_{22}^{(fd)} - i\Delta\bar{S}_{22}^{(fd)} = \sum_f (A_2 \delta k_f H_f) e^{i\theta_f} \end{cases}, \quad (4)$$

where

$$\begin{aligned} A_0 &= \frac{1}{R_E \sqrt{4\pi}}, \\ A_m &= \frac{(-1)^m}{R_E \sqrt{8\pi}}, \quad (m = 1, 2). \end{aligned} \quad (5)$$

$\theta_f(t) = \bar{n} \cdot \bar{\beta}(t)$ is the argument of respective tide constituent f . $\delta k_f = \delta k_f^R + i\delta k_f^I$ is the difference for a Love number from its nominal value on frequency f . H_f is the amplitude of the term on f , $\bar{\beta} = (\tau, s, h, p, N^l, p_s)$ is a six-vector of Doodson's fundamental arguments, \bar{n} is a six-vector of multipliers of the fundamental arguments, and (fd) denotes ‘‘frequency dependent’’. The detailed information about these terms and their computation is given in (Petit and Luzum 2010, Chapters 5 and 6).

Corrections to Stokes coefficients to account for effects of the ocean tides are expressed as

$$\Delta\bar{C}_{nm}^{(\text{ocean})} - i\Delta\bar{S}_{nm}^{(\text{ocean})} = \sum_f \sum_{\pm} (C_{f, nm}^{\pm} \mp iS_{f, nm}^{\pm}) e^{\pm i\theta_f}, \quad (6)$$

where $\theta_f = m(\theta_g + \pi) - \bar{N} \cdot \bar{F}$, $\bar{F} = (l, l', F, D, \Omega)$ is a five-vector of Delaunay variables of nutation theory, \bar{N} is a five-vector of multipliers of the Delaunay variables for the nutation of frequency ($-f + d\theta_g/dt$), θ_g is GMST (in angle units). $C_{f, nm}^{\pm}$ and $S_{f, nm}^{\pm}$ are the harmonic coefficients of the main waves of the ocean tides model FES2004 recommended for use by the IERS Conventions 2010. Their values can be taken from http://tai.bipm.org/iers/convupdt/convupdt_c6.html. Detailed information about the effect of ocean tides on the geopotential is given in (Petit and Luzum 2010, Section 6.3).

3.2.2 DE tidal model: direct acceleration with five time delays

The full description of the model used in the DE430 ephemeris can be found in (Folkner et al. 2014, Section III.C). The acceleration of the Moon is evaluated separately for the tides raised by the Sun and the Moon itself, on three frequencies: zonal (i.e. due to variation of $C_{20, E}$), diurnal ($C_{21, E}$ and $S_{21, E}$), and semi-diurnal ($C_{22, E}$ and $S_{22, E}$). Each of the three frequencies has its fixed Love number k_{2m} . Tidal dissipation causes the response of the earth to be delayed. Consequently, the perturbing acceleration from a tide-raising body at order m at time t is derived from Eq. (1) using tidal response $\Delta\bar{C}_{2m, E}$, $\Delta\bar{S}_{2m, E}$ created by the body at time $t - \tau_{mO}$ at the Earth rotated back to time $t - \tau_{mR}$. Pragmatically, the terrestrial phase shifts depend on tidal period and the two extra delays τ_{1O} and τ_{2O} allow the diurnal and semidiurnal tidal phases to vary linearly with frequency (Williams and Boggs 2016).

We denote $\mathbf{r}(t)$ the geocentric position of the Moon. The tidal distortion for each order is computed by replacing the geocentric position of the tide-raising body $\mathbf{r}_{\text{body}}(t)$ with $\mathbf{r}_m^* = R_z(\dot{\theta}_E \tau_{mR}) \mathbf{r}_{\text{body}}(t - \tau_{mO})$, where $\dot{\theta}_E$ is the Earth's sidereal rotation rate. We break down the vectors to ‘‘equatorial’’ and ‘‘polar’’ components with respect to the Earth's equator: $\mathbf{r} = \boldsymbol{\rho} + \mathbf{z}$, $\mathbf{r}_m^* = \boldsymbol{\rho}_m^* + \mathbf{z}_m^*$. Parameters with an asterisk are used for calculating the tide. The equation for the perturbing acceleration of the Moon is:

$$\begin{aligned} \frac{\Delta\mathbf{f}}{m} = \frac{3\mu_j}{2} \left(\frac{R_E}{r}\right)^5 & \left[\frac{k_{20}}{r_0^{*5}} \left((2z_0^{*2} \mathbf{z} + \rho_0^{*2} \boldsymbol{\rho}) - 5 \frac{(zz_0^*)^2 + \frac{1}{2}(\rho\rho_0^*)^2}{r^2} \mathbf{r} + r_0^{*2} \mathbf{r} \right) \right. \\ & + \frac{k_{21}}{r_1^{*5}} \left(2((\boldsymbol{\rho} \cdot \boldsymbol{\rho}_1^*) \mathbf{z}_1^* + zz_1^* \boldsymbol{\rho}_1^*) - \frac{10zz_1^*(\boldsymbol{\rho} \cdot \boldsymbol{\rho}_1^*) \mathbf{r}}{r^2} \right) \\ & \left. + \frac{k_{22}}{r_2^{*5}} \left(2(\boldsymbol{\rho} \cdot \boldsymbol{\rho}_2^*) \boldsymbol{\rho}_2^* - \rho_2^{*2} \boldsymbol{\rho} - 5 \frac{(\boldsymbol{\rho} \cdot \boldsymbol{\rho}_2^*)^2 - \frac{1}{2}(\rho\rho_2^*)^2}{r^2} \mathbf{r} \right) \right], \quad (7) \end{aligned}$$

where μ_j is the gravitational parameter of the tide-raising body, and R_E is Earth's equatorial radius. The acceleration is given in the inertial frame for one tide-raising body; to get the total perturbing geocentric acceleration of the Moon, one has to

add up the results of Eq. (7) with the Moon and the Sun as the tide-raising bodies, and then multiply by $(1 + \mu_M/\mu_E)$.

Zonal tides do not depend on the rotation of the Earth, so $\tau_{0R} = 0$. Other rotational delays, τ_{1R} and τ_{2R} , are determined from observations. Love numbers and orbit delays are fixed to match the most influential solid Earth tides and ocean tides from known models. Values used in this work are $k_{20} = 0.335$, $k_{21} = 0.320$, $k_{22} = 0.282$, $\tau_{0O} = 0.0780$ d, $\tau_{1O} = -0.044$ d, and $\tau_{2O} = -0.113$ d. Those values are modified from the ones used in DE430, but note $k_{22}\tau_{2O} = -0.031866$ is about the same as for DE430 ($0.320 \times -0.1 = -0.032$).

The negative values of τ_{mO} reflect the increase of ocean phase shift with period rather than a response to the future position of the Moon. The negative τ_{1O} reflects the increase in the diurnal phase lag between the O1 and Q1 tides, while the negative τ_{2O} reflects the increase in the semidiurnal phase lag between the M2 and N2 tides. For details, we refer to (Williams and Boggs 2016, Section 4).

3.3 Lunar frame

The lunar frame is aligned with the principal axes of the undistorted lunar mantle. The orientation of the lunar frame w.r.t. the inertial frame is determined by three Euler angles: ϕ , θ , and ψ that evolve over time. The transformation from the lunar frame to the inertial frame is given by the matrix:

$$R_{L2C}(t) = R_z(\phi(t))R_x(\theta(t))R_z(\psi(t)). \quad (8)$$

R_x and R_z are matrices of right-hand rotations around axes x and z , respectively. The argument t will be omitted when appropriate.

Instantaneous rates of the Euler angles at time t are denoted $\dot{\phi}(t)$, $\dot{\theta}(t)$, and $\dot{\psi}(t)$. Let $\boldsymbol{\omega}(t)$ be the angular velocity of the mantle, referred to the lunar frame:

$$\begin{aligned} \omega_x &= \dot{\phi} \sin \theta \sin \psi + \dot{\theta} \cos \psi \\ \omega_y &= \dot{\phi} \sin \theta \cos \psi - \dot{\theta} \sin \psi \\ \omega_z &= \dot{\phi} \cos \theta + \dot{\psi} \end{aligned} \quad (9)$$

The behavior of the lunar mantle depends on $\dot{\boldsymbol{\omega}}(t)$ and obeys the following second derivatives of the Euler angles (Standish et al. 1992):

$$\begin{aligned} \ddot{\phi} &= \frac{\dot{\omega}_x \sin \psi + \dot{\omega}_y \cos \psi + \dot{\theta}(\dot{\psi} - \dot{\phi} \cos \theta)}{\sin \theta} \\ \ddot{\theta} &= \dot{\omega}_x \cos \psi - \dot{\omega}_y \sin \psi - \dot{\phi} \dot{\psi} \sin \theta \\ \ddot{\psi} &= \dot{\omega}_z - \ddot{\phi} \cos \theta + \dot{\phi} \dot{\theta} \sin \theta \end{aligned} \quad (10)$$

$\dot{\boldsymbol{\omega}}(t)$, in turn, depends on the torque $\mathbf{N}(t)$. Using the Euler's equation for the angular momentum in a rotating reference frame ($\mathbf{N} = \dot{\mathbf{L}} + \boldsymbol{\omega} \times \mathbf{L}$, where $\mathbf{L} = I\boldsymbol{\omega}$ is the angular momentum in the rotating frame), we can write $\dot{\boldsymbol{\omega}}(t)$ in the following form:

$$\dot{\boldsymbol{\omega}} = \left(\frac{I}{m}\right)^{-1} \left[\frac{\mathbf{N}}{m} - \frac{\dot{I}}{m} \boldsymbol{\omega} - \boldsymbol{\omega} \times \left(\frac{I}{m} \boldsymbol{\omega}\right) \right] \quad (11)$$

where m is the mass of the Moon, and $I(t)$ is the inertia tensor of the lunar mantle. The torque \mathbf{N} (also referred to the lunar frame) is calculated as:

$$\frac{\mathbf{N}}{m} = \sum_{A \neq M} \frac{\mathbf{N}_{\text{figM-pmA}}}{m} + \frac{\mathbf{N}_{\text{figM-figE}}}{m} + \frac{\mathbf{N}_{\text{cmb}}}{m}, \quad (12)$$

where $\mathbf{N}_{\text{figM-pmA}}(t)$ is a torque from point-mass A to the Moon's figure:

$$\frac{\mathbf{N}_{\text{figM-pmA}}}{m} = (\mathbf{r}_M - \mathbf{r}_A) \times \frac{\mathbf{f}_{\text{figM-pmA}}}{m}, \quad (13)$$

where $\mathbf{f}_{\text{figM-pmA}}(t)$ is the force acting on the point-mass in the Moon's gravitational field (see Eq. 1). The following point-masses are taken into account: Earth, Sun, Venus, Mars, Jupiter.

$\mathbf{N}_{\text{figM-figE}}(t)$ is a torque from the Earth's oblateness to the Moon's figure:

$$\begin{aligned} \frac{\mathbf{N}_{\text{figM-figE}}}{m} = \frac{15\mu_E R_E^2 J_{2E}}{2r_{\text{EM}}^5} & \left[\left(1 - 7(\hat{\mathbf{r}}_{\text{EM}} \cdot \hat{\mathbf{p}})^2\right) \left(\hat{\mathbf{r}}_{\text{EM}} \times \frac{I}{m} \hat{\mathbf{r}}_{\text{EM}}\right) \right. \\ & + 2(\hat{\mathbf{r}}_{\text{EM}} \cdot \hat{\mathbf{p}}) \left(\hat{\mathbf{r}}_{\text{EM}} \times \frac{I}{m} \hat{\mathbf{p}} + \hat{\mathbf{p}} \times \frac{I}{m} \hat{\mathbf{r}}_{\text{EM}}\right) \\ & \left. - \frac{2}{5} \left(\hat{\mathbf{p}} \times \frac{I}{m} \hat{\mathbf{p}}\right) \right], \quad (14) \end{aligned}$$

where J_{2E} is Earth's oblateness factor, $r_{\text{EM}}(t)$ is Earth-Moon distance, $\hat{\mathbf{r}}_{\text{EM}}(t)$ is the normalized direction vector from the Moon to the Earth, and $\hat{\mathbf{p}}(t)$ is the direction of Earth's pole. All vectors in the equation are referred to the lunar frame.

\mathbf{N}_{cmb} will be explained in section 3.5.

3.4 Lunar inertia tensor

The inertia tensor of the lunar mantle is subject to delayed tidal distortion from Earth and delayed spin distortion. We refer to (Williams et al. 2001) and (Folkner et al. 2014) for full descriptions, while reproducing the equation here in its condensed form:

$$\begin{aligned} \frac{I}{m} = \frac{2R_M^2 \tilde{J}_2}{2\beta - \gamma + \beta\gamma} & \begin{bmatrix} 1 - \beta\gamma & 0 & 0 \\ 0 & 1 + \gamma & 0 \\ 0 & 0 & 1 + \beta \end{bmatrix} - \frac{I_c}{m} \\ & - k_2 \frac{\mu_E}{\mu_M} \left(\frac{R_M}{r}\right)^5 \begin{bmatrix} x^2 - \frac{1}{3}r^2 & xy & xz \\ xy & y^2 - \frac{1}{3}r^2 & yz \\ xz & yz & z^2 - \frac{1}{3}r^2 \end{bmatrix} \\ & + k_2 \frac{R_M^5}{3\mu_M} \begin{bmatrix} \omega_x^2 - \frac{1}{3}(\omega^2 - n^2) & \omega_x \omega_y & \omega_x \omega_z \\ \omega_x \omega_y & \omega_y^2 - \frac{1}{3}(\omega^2 - n^2) & \omega_y \omega_z \\ \omega_x \omega_z & \omega_y \omega_z & \omega_z^2 - \frac{1}{3}(\omega^2 + 2n^2) \end{bmatrix}, \quad (15) \end{aligned}$$

where R_M is the equatorial radius of the Moon; \tilde{J}_2 is the oblateness factor of the undistorted Moon; k_2 is the degree-2 Love number of the Moon; $\mathbf{r} = (x, y, z)^T$ is

the position of the Moon relative to Earth; n is the lunar mean motion. $I_c(t)$ is the inertia tensor of the liquid core that is explained in section 3.5. Tidal and spin distortions are evaluated with a delayed argument: calculation of $I(t)$ involves not $\mathbf{r}(t)$ and $\boldsymbol{\omega}(t)$, but $\mathbf{r}(t - \tau)$ and $\boldsymbol{\omega}(t - \tau)$.

The distortion of the lunar mantle affects its gravitational potential. The following equations describe how unnormalized spherical harmonic coefficients vary over time:

$$\begin{aligned}
C_{20} &= \frac{1}{R_M^2} \left[\frac{1}{2} \left(\frac{I_{11}^*}{m} + \frac{I_{22}^*}{m} \right) - \frac{I_{33}^*}{m} \right] \\
C_{22} &= \frac{1}{4R_M^2} \left[\frac{I_{22}^*}{m} - \frac{I_{11}^*}{m} \right] \\
C_{21} &= C_{21}^{(0)} - \frac{1}{R_M^2} \frac{I_{13}^*}{m} \\
S_{21} &= S_{21}^{(0)} - \frac{1}{R_M^2} \frac{I_{32}^*}{m} \\
S_{22} &= S_{22}^{(0)} - \frac{1}{2R_M^2} \frac{I_{21}^*}{m}
\end{aligned} \tag{16}$$

Here the matrix I^* is the combined inertia tensor: $I^* = I + I_c$. The DE430 lunar equations are built on assumption that the mantle frame is aligned with the principal axes of the whole Moon, so the constant mean values $C_{21}^{(0)}$, $S_{21}^{(0)}$, and $S_{22}^{(0)}$ should be zero. I^* then is the total inertia tensor of the Moon. However, in this work a preliminary attempt has been made to include a nonzero $S_{21}^{(0)}$, see section 5.1.

3.5 Lunar fluid core

The core is assumed to be rotating like a solid and constrained by the shape of the core-mantle boundary (CMB) at the interior of the mantle, with moment of inertia constant in the mantle frame (Folkner et al. 2014):

$$\frac{I_c}{m} = \alpha_c \frac{C_T}{m} \begin{bmatrix} 1 - f_c & 0 & 0 \\ 0 & 1 - f_c & 0 \\ 0 & 0 & 1 \end{bmatrix}, \quad \frac{C_T}{m} = \frac{2(1 + \beta)}{2\beta - \gamma + \beta\gamma} R_M^2 \tilde{J}_2, \tag{17}$$

where α_c is a dimensionless coefficient for the ratio of core to total polar moments of inertia and f_c is the oblateness of the fluid core. C_T is the undistorted polar moment of inertia.

The orientation of the core is not important for the equations of the mantle—only its angular velocity $\boldsymbol{\omega}_c(t)$ is. The evolution of $\boldsymbol{\omega}_c$ is described by its time derivative, given in the mantle frame:

$$\dot{\boldsymbol{\omega}}_c = \left(\frac{I_c}{m} \right)^{-1} \left[-\boldsymbol{\omega} \times \frac{I_c}{m} \boldsymbol{\omega}_c - \frac{\mathbf{N}_{\text{cmb}}}{m} \right] \tag{18}$$

$\mathbf{N}_{\text{cmb}}(t)$ is the torque on the mantle due to the interaction with the fluid core. It is expressed in the mantle frame as:

$$\frac{\mathbf{N}_{\text{cmb}}}{m} = \frac{C_T}{m} \left[\frac{k_v}{C_T} (\boldsymbol{\omega}_c - \boldsymbol{\omega}) + \alpha_c f_c (\hat{\mathbf{z}} \cdot \boldsymbol{\omega}_c) (\hat{\mathbf{z}} \times \boldsymbol{\omega}_c) \right], \tag{19}$$

where $\frac{k_w}{C_T}$ is a friction parameter (measured in day^{-1}), and $\hat{\mathbf{z}} = (0, 0, 1)^T$.

4 Reductions of observations

The calculation of modeled light travel time requires solving a system of equations:

$$\begin{cases} t_2 - t_1 = \frac{|\mathbf{l}_{\text{BCRS}}(t_2) - \mathbf{s}_{\text{BCRS}}(t_1)|}{c} + \Delta_{\text{grav}}(t_1, t_2) + \Delta_{\text{atm}}(t_1, t_2) \\ t_3 - t_2 = \frac{|\mathbf{s}_{\text{BCRS}}(t_3) - \mathbf{l}_{\text{BCRS}}(t_2)|}{c} + \Delta_{\text{grav}}(t_3, t_2) + \Delta_{\text{atm}}(t_3, t_2) \end{cases} \quad (20)$$

t_1 , t_2 , and t_3 are the times of emission, reflection, and reception of the signal in the TDB timescale. Usually, a normal point contains t_1 in UTC, which requires converting it to TDB and then solving (20) w.r.t. t_2 and t_3 . $\mathbf{s}_{\text{BCRS}}(t_i)$ and $\mathbf{l}_{\text{BCRS}}(t_i)$ are the positions of the station and the lunar reflector at time t_i in the inertial frame. Δ_{grav} is the relativistic gravitational delay of signal propagation, while Δ_{atm} is the tropospheric delay.

Calculation of the position of the station in the inertial frame should include a relativistic transformation from geocentric to barycentric coordinate systems (Petit and Luzum 2010, eq. 11.19):

$$\mathbf{s}_{\text{BCRS}} = \mathbf{r}_E + \mathbf{s}_{\text{GCRS}} \left(1 - \frac{U_E}{c^2} - L_C \right) - \frac{1}{2} \left(\frac{\dot{\mathbf{r}}_E \cdot \mathbf{s}_{\text{GCRS}}}{c^2} \right) \dot{\mathbf{r}}_E \quad (21)$$

where $U_E(t)$ is the gravitational potential at the geocenter, excluding the Earth's mass, $\mathbf{r}_E(t)$ and $\dot{\mathbf{r}}_E(t)$ are the barycentric position and velocity of the Earth, and $L_C = 1.48082686741 \times 10^{-8}$.

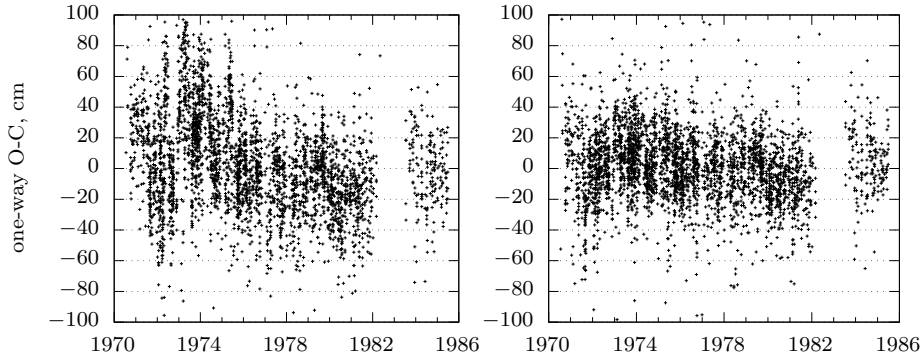
Calculation of inertial geocentric position of the station should account for Earth's rotation, pole tides, and solid body and ocean loading tides:

$$\mathbf{s}_{\text{GCRS}} = R_{\text{T2C}} (\mathbf{s}_{\text{TRS}} + \mathbf{\Delta}_{\text{pole}} + \mathbf{\Delta}_{\text{solid}} + \mathbf{\Delta}_{\text{ocean}}). \quad (22)$$

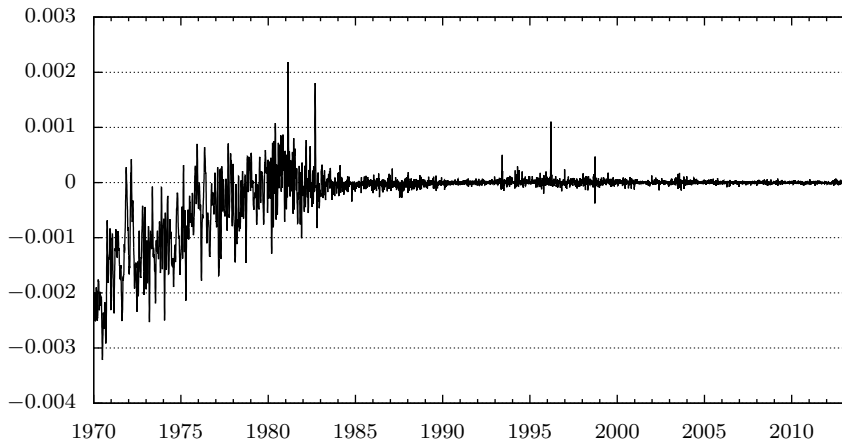
where $\mathbf{s}_{\text{TRS}}(t)$ is the position of the station in the terrestrial reference frame, adjusted for the drift.

Note: the Haleakala station had its receiving telescope ($\mathbf{s}_{\text{TRS}}(t_3)$) located at some distance from the laser ($\mathbf{s}_{\text{TRS}}(t_1)$), so that there are two different \mathbf{s}_{TRS} in the equations. The displacement between the telescope and the laser is not determined from the observations; the position of the laser is determined, while the position of the telescope is calculated from its known displacement that can be found in (Newhall et al. 1990).

The transformation R_{T2C} from the TRS to GCRS frame is done strictly in accordance with IAU 2000/2006 resolutions. The algorithms for the transformation can be found in (Petit and Luzum 2010, Chapter 6). Unmodeled celestial pole offsets $dX(t)$ and $dY(t)$ and terrestrial pole coordinates $(x_{\text{pole}}(t), y_{\text{pole}}(t))$ were taken from the published IERS C04 solution (Bizouard and Gambis 2009, 2011) which is combined from SLR, GPS, and VLBI data, including the observations from the QUASAR network (Finkelstein et al. 2012). However, the C04 solution gave poor results for observations made before 1982 (the only station from which we have data for that time is McDonald). The decision has been made to use the JPL KEOF series (<http://keof.jpl.nasa.gov/>) for early observations. Figure 1 shows the postfit residuals of the McDonald observations obtained using C04 (one-way wrms 30.8 cm) and KEOF (one-way wrms 20.1 cm).

Fig. 1 Postfit O-C of the McDonald observations using C04 (left) and KEOF (right)

The reason for KEOF giving better results can be that the variation of latitude (VOL) and UT0 determined from LLR observations were part of the KEOF solution (Ratcliff and Gross 2015); besides, the C04 series has $dX = dY = 0$ before 1984. Since 1984, C04 and KEOF give equally good results for all stations (there is almost no LLR data between 1982 and 1984). Figure 2, showing the difference between the KEOF and C04 series of UT1, confirms that the two solutions came close enough to each other starting around 1984.

Fig. 2 $UT1_{\text{KEOF}} - UT1_{\text{C04}}$, seconds

For $\Delta_{\text{pole}}(t)$, $\Delta_{\text{solid}}(t)$, and $\Delta_{\text{ocean}}(t)$, we refer to the respective sections of (Petit and Luzum 2010): 7.1.1 (solid Earth tide), 7.1.2 (ocean loading tide), and 7.1.4 (pole tide). Atmospheric pressure loading and ocean pole tide loading are not handled in this work.

The position of the lunar reflector has to be transformed from the lunar frame to the inertial frame, similar to the position of the station:

$$\begin{aligned} \mathbf{l}_{\text{BCRS}} &= \mathbf{r}_M + \mathbf{l}_{\text{LCRS}} \left(1 - \frac{U_M}{c^2} \right) - \frac{1}{2} \left(\frac{\dot{\mathbf{r}}_M \cdot \mathbf{l}_{\text{LCRS}}}{c^2} \right) \dot{\mathbf{r}}_M \\ \mathbf{l}_{\text{LCRS}} &= R_{\text{L2C}} \mathbf{l}_{\text{PA}} + \Delta_{\text{solidmoon}}^{(E)} + \Delta_{\text{solidmoon}}^{(S)} \end{aligned} \quad (23)$$

where $U_M(t)$ is the gravitational potential at the Moon's center, excluding the Moon's mass, $\mathbf{r}_M(t)$ and $\dot{\mathbf{r}}_M(t)$ are the barycentric position and velocity of the Moon, \mathbf{l}_{PA} is the position of the reflector in the lunar frame (principal axes), and $\Delta_{\text{solidmoon}}^{(E)}(t)$ and $\Delta_{\text{solidmoon}}^{(S)}(t)$ are displacements due to solid Moon tide raised by Earth and Sun, respectively. A simple model of solid Moon tides was used in this work, while more detailed models have been recently developed; see (Williams and Boggs 2015).

The equation of the tide involves the degree-2 Love number h_2 and the degree-2 Shida number l_2 (Petit and Luzum 2010, eq. 7.5):

$$\begin{aligned} \Delta_{\text{solidmoon}} &= \frac{\mu_A R_M^4}{\mu_M r_{\text{MA}}^3} \left[\frac{h_2}{2} \left(3 \left(\hat{\mathbf{r}}_{\text{MA}} \cdot \hat{\mathbf{l}} \right)^2 - 1 \right) \hat{\mathbf{r}}_{\text{MA}} + \right. \\ &\quad \left. 3l_2 \left(\hat{\mathbf{r}}_{\text{MA}} \cdot \hat{\mathbf{l}} \right) \left(\hat{\mathbf{r}}_{\text{MA}} - \left(\hat{\mathbf{r}}_{\text{MA}} \cdot \hat{\mathbf{l}} \right) \hat{\mathbf{l}} \right) \right], \end{aligned} \quad (24)$$

where $\hat{\mathbf{l}} = R_{\text{L2C}} \hat{\mathbf{l}}_{\text{PA}}$ is the unit vector of the reflector rotated to the inertial frame, $\mathbf{r}_{\text{MA}} = \mathbf{r}_A - \mathbf{r}_M$ is the position of the tide-raising body relative to the Moon, and $\hat{\mathbf{r}}_{\text{MA}}$ is the respective unit vector.

Calculation of Δ_{atm} is done using a combination of two empirical models: zenith delay (Mendes and Pavlis 2004) and mapping function (Mendes et al. 2002). For the calculation of Δ_{grav} , a theoretical result is used that can be found for instance in (Kopeikin 1990). Delays from the following point-masses are added up: Sun, Earth, Moon, Jupiter, Saturn.

The observed ranges are given in UTC timescale, so the resulting ‘‘computed’’ observation should be transformed from the TDB timescale to TT and then to UTC. From February 1968 till the end of 1971, UTC ran faster than TT by the factor of $(1 + 3 \times 10^{-8})$. Since 1972, UTC and TT have the same rate, while UTC has jumps. Given that the earliest LLR observations were made in 1969, and that no LLR normal point has t_1 and t_3 on different sides of a UTC jump, we can assume that $(t_3 - t_1)^{(\text{UTC})} = (t_3 - t_1)^{(\text{TT})} / (1 + \zeta)$, where $\zeta = 3 \times 10^{-8}$ before 1972 and zero since 1972. The complete transformation from TDB to UTC will be:

$$\begin{aligned} C &= [t_3 - t_1 + \text{TTminusTDB}(t_3, \mathbf{s}_{\text{GCRS}}(t_3)) - \\ &\quad \text{TTminusTDB}(t_1, \mathbf{s}_{\text{GCRS}}(t_1))] / (1 + \zeta) + \frac{b}{c} \end{aligned} \quad (25)$$

For calculating (TT – TDB) at time t and point $\mathbf{s}_{\text{GCRS}}(t)$, a theoretical equation is used, which can be found for instance in (Folkner et al. 2014, eq. 5). The geocentric terms of the equation are integrated along with the Solar system equations and stored in ephemeris; just one topocentric term is taken into account in Eq. (25): $(\dot{\mathbf{r}}_E(t) \cdot \mathbf{s}_{\text{GCRS}}(t)) / c^2$.

The bias b is a determined parameter and is specific to a station and to a certain period of time. The list of biases applied in this work can be found in section 5.2.3.

5 Determined and fixed parameters

Some of the parameters used in this model, like the positions of the lunar reflectors, are to be determined from LLR exclusively. Other parameters, like the ones of the orientation of the Earth, are assumed to be determined from VLBI and GNSS observations with better accuracy than they could have possibly been determined from LLR.

5.1 Borderline parameters

There are choices regarding parameters that can be determined either from LLR or alternative techniques. Such parameters are:

- Spherical harmonics of the lunar gravitational potential can be determined from LLR or from the observations made during the GRAIL spacecraft mission (Konopliv et al. 2013)
- the mass of the Moon can be determined from LLR (given the mass of the Earth from some other solution), or from GRAIL.
- tidal parameters of the Moon (h_2 , k_2 , l_2) can be determined from LLR or taken from GRAIL (Williams et al. 2014) or other solutions.
- parameters of tidal variations of the Earth's gravitational potential can be determined from LLR or gravimetry and altimetry measurements (the latter is the basis of the model recommended in the IERS Conventions).
- drift of the stations can be determined from LLR or GNSS observations.

Lunar \tilde{J}_2 , k_2 and l_2 in this work were fixed to the values determined from GRAIL, while h_2 was determined from LLR. $\mu_E + \mu_M$ was determined from LLR too, while $\frac{\mu_E}{\mu_M}$ was fixed to the value determined from spacecraft observations.

GRAIL's undistorted value of \bar{C}_{22} was left out: following Eq. (16), $C_{22}(t)$ is calculated dynamically with β and γ as determined parameters. Undistorted (mean) values $C_{21}^{(0)}$, $S_{21}^{(0)}$, and $S_{22}^{(0)}$ are fixed to zero in DE430, so that the mantle frame is aligned with the principal axes. The nonzero values of \bar{C}_{21} , \bar{S}_{21} , and \bar{S}_{22} in the GRAIL's solution are a sign of misalignment caused by inner structure of the Moon. Currently, there is no model explaining this misalignment, and since the present theory has Eqs. (15) and (16) in the PA frame, it makes little sense to just set $C_{21}^{(0)}$, $S_{21}^{(0)}$, and $S_{22}^{(0)}$ based on the use GRAIL's values \bar{C}_{21} , \bar{S}_{21} , and \bar{S}_{22} . However, a separate solution was obtained in this work, to test how the dynamical system behaves with $S_{21}^{(0)}$ taken from GL660b.

The physical processes in the lunar core, mantle, and the core-mantle boundary seem to have yet-unmodeled effects that can be presented in the form of empirical correction of lunar gravitational potential coefficients. By trial and error, it has been found that fitting \bar{C}_{32} , \bar{S}_{32} , and \bar{C}_{33} to observations gives better results.

The DE430 and IERS 2010 tidal models (see subsections 3.2.1 and 3.2.2) were both implemented in this work, and a solution was obtained with each.

The drift of stations was modeled as linear motion in a cylindrical coordinate system $(\lambda, r \cos \phi, r \sin \phi)$. The choice of the coordinate system was historical; while it is not strictly consistent with the IERS Conventions, where tectonic plate motions are modeled with linear function in cartesian coordinates, the nonlinearities on relatively short timespans, used in this work, are very small and can be ignored.

For stations that have been doing LLR for decades—McDonald/MRS1/MLRS2 and CERGA—the velocities were fit to the observations. Velocities of Haleakala and Matera can not be determined from LLR with good confidence, as they have relatively short timespans of LLR observations; but they are equipped with GPS receivers, which allowed taking their velocities from a global GNSS solution for the terrestrial frame.

The International GNSS Service (IGS) provides weekly combined coordinate solutions for IGS stations network (Ferland and Piraszewski 2009). Every solution is the result of a combination of independent estimates of solutions provided by different IGS Analysis Centers. Coordinates are aligned to IGS realizations of ITRF. Details and links to data are available at IGS website <http://igs.cb.jpl.nasa.gov/components/prods.html>. To get velocities of stations we have fit all of the coordinate time-series for considered stations to a linear model of movement.

The Apache Point station is not a part of any ITRF solution (it does not possess a GPS receiver). The closest station to Apache Point that is present in the ITRF2014 solution is White Sands (WSMN, 65 km away); but it is located on the desert floor, while Apache Point is in the mountains. The decision has been made to take the velocity of a GPS station P027 (2.5 km away from Apache Point) from a PBO solution given in the IGS08 frame (ftp://data-out.unavco.org/pub/products/velocity/pbo.final_igs08.vel). In future work, when more Apache Point observations are processed, detecting its velocity from LLR observations can be considered.

5.2 Special parameters for unmodeled effects

5.2.1 Longitude libration

The DE430 lunar theory includes three additional periodic terms for longitude libration to account for small effects related to frequency dependent tidal dissipation (Williams et al. 2013).

$$\Delta\lambda = A_1 \cos l' + A_2 \cos(2l - 2D) + A_3 \cos(2F - 2l). \quad (26)$$

The equation involves Delaunay arguments: lunar mean anomaly l , solar mean anomaly l' , argument of latitude F , and elongation of Moon from Sun D . A_1 , A_2 , and A_3 are the special parameters to be determined from observations.

The lunar mantle is supposed to have an unmodeled libration in longitude by the periodic $\Lambda(t)$ in the MER (mean Earth – mean rotation) frame. This is equal to the following rotation in our chosen PA (principal axes) frame:

$$R_{\text{libr}}(\Lambda) = R_x(-\delta_x)R_y(-\delta_y)R_z(\Lambda)R_y(\delta_y)R_x(\delta_x), \quad (27)$$

where constant angles δ_x and δ_y are derived from an ephemeris to match the transformation from the MER frame to the PA frame. In DE430 (Folkner et al. 2014), $\delta_x = 0.285''$ and $\delta_y = 78.580''$. In this work, a simplification has been made: $R_{\text{libr}}(\Lambda) \approx R_z(\Lambda)$, since the change of axis (PA Z instead of MER Z) brings just sub-millimeter differences of calculated ranges. Thus, the total lunar rotation matrix becomes $R_{L2C} = R_z(\phi)R_x(\theta)R_z(\psi + \Lambda)$.

5.2.2 Extra eccentricity rate

Tidal dissipation effects in Earth and Moon cause a secular growth of eccentricity of the orbit of the Moon. The eccentricity rate derived from DE430 (Williams et al. 2013) is 1.36×10^{-11} /yr. An extra eccentricity rate is determined to detect unmodeled (tidal or other) effects in the orbit of the Moon. From (Chapront-Touzé and Chapront 1998), we know the effect on the Earth-Moon distance $A(t)$ with the Delaunay arguments:

$$A = 385000.5 - 20905.4 \cos l - 3699.1 \cos(2D - l) - \dots \text{ km.} \quad (28)$$

Since the terms with the l argument have a hidden e (eccentricity) in the coefficient, we can derive

$$dA/de \approx -\frac{20905.4}{e} \cos l - \frac{3699.1}{e} \cos(2D - l) \approx -380791 \cos l - 67379 \cos(2D - l). \quad (29)$$

Multiplying the dA/de by the time of the observation since the epoch, we get the approximate partial of the one-way laser range w.r.t. extra de/dt .

5.2.3 Biases

Biases are determined parameters intended to compensate changes in station's equipment or other anomalies. Table 3 lists biases used in this work; this set is close to the one used during building the DE430 ephemerides. Different biases have different origins.

Biases 14, 15, and 16 are known from the changes in calibration and ranging rings at the Haleakala station (see Table 4; while the last two changes did not create any detectable bias). Similarly, biases 6, 7, and 12 match upgrades of the laser at the CERGA station (Ruby→YAG→MeO). Biases 1, 4, and 5 come from known changes at the Apache Point station (the installation of a new detector in November 2010; different calibration technique since April 2012). Biases 13, 21, 27 and 28 cover the whole timespan of their stations' operation. Other biases have no known cause (one can guess a human error) and were detected in post-fit residuals.

5.3 Full list of parameters

The full list of parameters, fixed or fit, used in different solutions in this work, is given in Table 5. The chosen epoch for determined initial values is that of the EPM ephemeris: JD 2446000.5, except for stations' positions: their epochs were chosen individually. Table 6 summarizes the stations' parameters.

6 Software used in this work

ERA (Ephemeris Research in Astronomy), version 8 was used for processing the observations, refining the parameters and integrating the dynamical equations (Pavlov and Skripnichenko 2015), ERA comprises a domain-specific language

#	Station	from	to	#	Station	from	to
1	Apache	07.04.2006	01.11.2010	15	Haleakala	02.04.1986	30.07.1987
2	Apache	15.12.2007	30.06.2008	16	Haleakala	31.07.1987	14.08.1987
3	Apache	20.09.2008	20.06.2009	17	Haleakala	09.06.1985	10.06.1985
4	Apache	01.11.2010	07.04.2012	18	Haleakala	28.01.1989	29.01.1989
5	Apache	07.04.2012	02.09.2013	19	Haleakala	23.08.1989	24.08.1989
6	CERGA	01.06.1984	13.06.1986	20	Haleakala	06.02.1990	01.09.1990
7	CERGA	01.10.1987	01.08.2005	21	McDonald	01.01.1969	01.07.1985
8	CERGA	10.12.1996	18.01.1997	22	McDonald	01.12.1971	05.12.1972
9	CERGA	08.02.1997	24.06.1998	23	McDonald	21.04.1972	27.04.1972
10	CERGA	04.12.2004	07.12.2004	24	McDonald	18.08.1974	16.10.1974
11	CERGA	03.01.2005	06.01.2005	25	McDonald	05.10.1975	01.03.1976
12	CERGA	01.11.2009	01.01.2014	26	McDonald	01.12.1983	17.01.1984
13	Haleakala	01.11.1984	01.09.1990	27	Matera	01.01.2003	01.01.2016
14	Haleakala	01.11.1984	01.04.1986	28	MLRS1	01.08.1983	28.01.1988

Table 3 Biases determined from LLR observations. Date notation is DD.MM.YYYY

Time span	Calibration rings	Ranging rings
04.10.1984 – 01.04.1986	2, 3, 4	1, 2, 3, 4
02.04.1986 – 30.07.1987	3	1, 2, 3, 4
31.07.1987 – 14.08.1987	3	3, 4
15.08.1987 – 09.11.1987	3	3
10.11.1987 – 18.02.1988	3, 4	3, 4
19.02.1988 – 31.08.1990	1, 2, 3, 4	1, 2, 3, 4

Table 4 Changes of equipment at the Haleakala station. Date notation is DD.MM.YYYY

SLON tailored for astronomical tasks (Krasinsky et al. 1988). ERA-8 is a rework of earlier versions of ERA (Krasinsky and Vasilyev 1997, 2006). Unlike the earlier versions, ERA-8 is based on the Racket programming platform (Findler et al. 2002; Flatt and PLT 2010). and has SQLite (<http://sqlite.org>) as the database engine. Most of the numerical algorithms of ERA-8 are implemented in C.

SOFA library (Hohenkerk 2012; <http://www.iausofa.org>) was used for calculation of the precession-nutation matrix according to IAU2000/2006 model, conversion of time scales, calculation of Delaunay arguments, and conversion between geocentric and geodetic coordinates.

For optical zenith delay (Mendes and Pavlis 2004) and mapping function (Mendes et al. 2002), FCULZD_HPA and FCUL_A routines were used. Station displacement due to solid tides (Mathews et al. 1997) was calculated with the DEHANTTIDEINEL package. For ocean tides, HARDISP package was used; files with ocean loading coefficients for specific stations were downloaded from the Onsala Space Observatory website (<http://holt.oso.chalmers.se/loading/>).

For numerical integration, an implementation of Gauss-Everhart algorithm from (Avdyushev 2010) was used, but rewritten from Fortran to C and modified to use extended precision floating-point numbers (80-bit) instead of double precision (64-bit).

Notation	parameter	type	notes
μ_S	standard gravitational parameter of the Sun	fixed	fixed to DE430 value in this work; may differ in the EPM ephemeris
μ_E/μ_M	Earth-Moon mass ratio	fixed	determined from spacecraft observations; fixed to DE430 value in this work, may differ in EPM
$\mu_E + \mu_M$	standard gravitational parameter of the E-M system	fit	
$C_{nm,E}, S_{nm,E}$	spherical harmonic coefficients of Earth's gravitational potential	fixed	up to $n_{\max} = 6$, taken from model based on EGM2008, see section 6.1 of Conventions; DE tidal model comes with an altered $\tilde{C}_{20,E}$
k_{20}, k_{21}, k_{22}	potential degree-2 Love numbers of Earth zonal, diurnal, and semi-diurnal tides	fixed	in DE tidal model: $k_{20} = 0.335$, $k_{21} = 0.320$, $k_{22} = 0.282$; IERS tidal model is more complex
$\tau_{0O}, \tau_{1O}, \tau_{2O}$	orbital delays of Earth zonal, diurnal, and semi-diurnal tides	fixed/absent	only in DE tidal model: $\tau_{0O} = 0.0780$ d, $\tau_{1O} = -0.044$ d, $\tau_{2O} = -0.113$ d
τ_{1R}, τ_{2R}	rotational delays of Earth diurnal, semi-diurnal tides	fit/absent	present only in DE tidal model
l_2, k_2	degree-2 lunar Shida number and Love number	fixed	taken from GRAIL results
h_2	degree-2 lunar radial displacement Love number	fit	
C_{20}	undistorted normalized main zonal lunar harmonic	fixed	taken from GRAIL (solution GL660b)
β, γ	ratios between undistorted main moments of inertia	fit	
C_{21}, S_{21}, S_{22}	other degree-2 harmonics	fixed	Zero; S_{21} taken from GL660b in one solution
C_{32}, S_{32}, C_{33}	some degree-3 harmonics	fit	
C_{nm}, S_{nm}	other lunar harmonics	fixed	taken from GL660b up to degree 6
τ	lunar tidal delay	fit	
f_c	oblateness of the lunar core	fit	
k_v/C_T	CMB interaction	fit	
α_c	core polar moment / undistorted total polar moment	fixed	DE430 fixed value 0.0007
A_1, A_2, A_3	unmodeled longitude libration amplitudes	fit	
$l_{PA} (\times 5)$	positions of five lunar retroreflectors	fit	
r_{EM}, \dot{r}_{EM}	position and velocity of the Moon w.r.t. Earth in the inertial frame at epoch	fit	
$\phi, \theta, \psi, \dot{\phi}, \dot{\theta}, \dot{\psi}$	Euler angles and their rates at epoch	fit	
$s_{TRS} (\times 7), \dot{s}_{TRS} (\times 5)$	positions and velocities of stations at their epochs	fixed/fit	see Table 6
ω_c	angular velocity of the lunar core at epoch	fit	
$b (\times 28)$	biases	fit	see Table 3
de/dt	extra eccentricity rate	fit/absent	present in some solutions

Table 5 Parameters used in dynamic model or reductions of observations

Parameter	type	notes
McDonald position	fit	epoch 01.01.1991
MLRS1 position	fit	epoch 01.01.1991
MLRS2 position	fit	epoch 01.01.1991
McDonald, MLRS1, MLRS2 velocity	fit	
Apache position	fit	epoch 01.06.2009
Apache velocity	fixed	GNSS solution (P027): $(-1.35, 0.03, -0.04)^T$ cm/yr
CERGA position	fit	epoch 01.01.2000
CERGA velocity	fit	
Haleakala position	fit	epoch 01.04.1986
Haleakala velocity	fixed	GNSS solution: $(-1.30, 6.16, 3.21)^T$ cm/yr
Matera position	fit	epoch 01.01.2008
Matera velocity	fixed	GNSS solution: $(-1.85, 1.86, 1.47)^T$ cm/yr

Table 6 Parameters of stations. Fixed velocities are given in cartesian coordinates

7 Results

7.1 Description of obtained solutions

Six solutions were obtained in this work. All the solutions are based on the same set of observations, while differing slightly in dynamical models and determined parameters.

- Solution I: DE tidal model, $\bar{C}_{21}^{(0)} = \bar{S}_{21}^{(0)} = \bar{S}_{22}^{(0)} = 0$, de/dt absent. This model is the closest match to the original DE430 model.
- Solution II: IERS tidal model, $\bar{C}_{21}^{(0)} = \bar{S}_{21}^{(0)} = \bar{S}_{22}^{(0)} = 0$, de/dt absent.
- Solution III: IERS tidal model, $\bar{C}_{21}^{(0)} = \bar{S}_{22}^{(0)} = 0$, $\bar{S}_{21}^{(0)}$ taken from GL660b, de/dt absent
- Solution Ie: same as solution I, but with de/dt fit.
- Solution Iie: same as solution II, but with de/dt fit.
- Solution IIIe: same as solution III, but with de/dt fit.

The main purpose of obtaining those solutions was to compare IERS and DE tidal models in terms of their fit to the LLR observations, and to see how they affect the extra eccentricity rate. Also, it was important to check whether the GL660b mean value of \bar{S}_{21} improves the overall results of LLR fits.

7.2 Difference in accelerations given by IERS and DE tidal models

Figure 3 shows periodic accelerations experienced by the Moon’s orbit in Solution I due to tidal perturbations from Earth. On the same orbit, the tidal accelerations obtained with the IERS model were calculated. The difference between DE and IERS accelerations (in the lunar frame) is shown on Figure 4. DE acceleration is permanently bigger on axis X (towards Earth) by some 0.02-0.03 mm/day². This may be due to the K1 tide that has a smaller Love number than the average k_{21} value used for DE430.

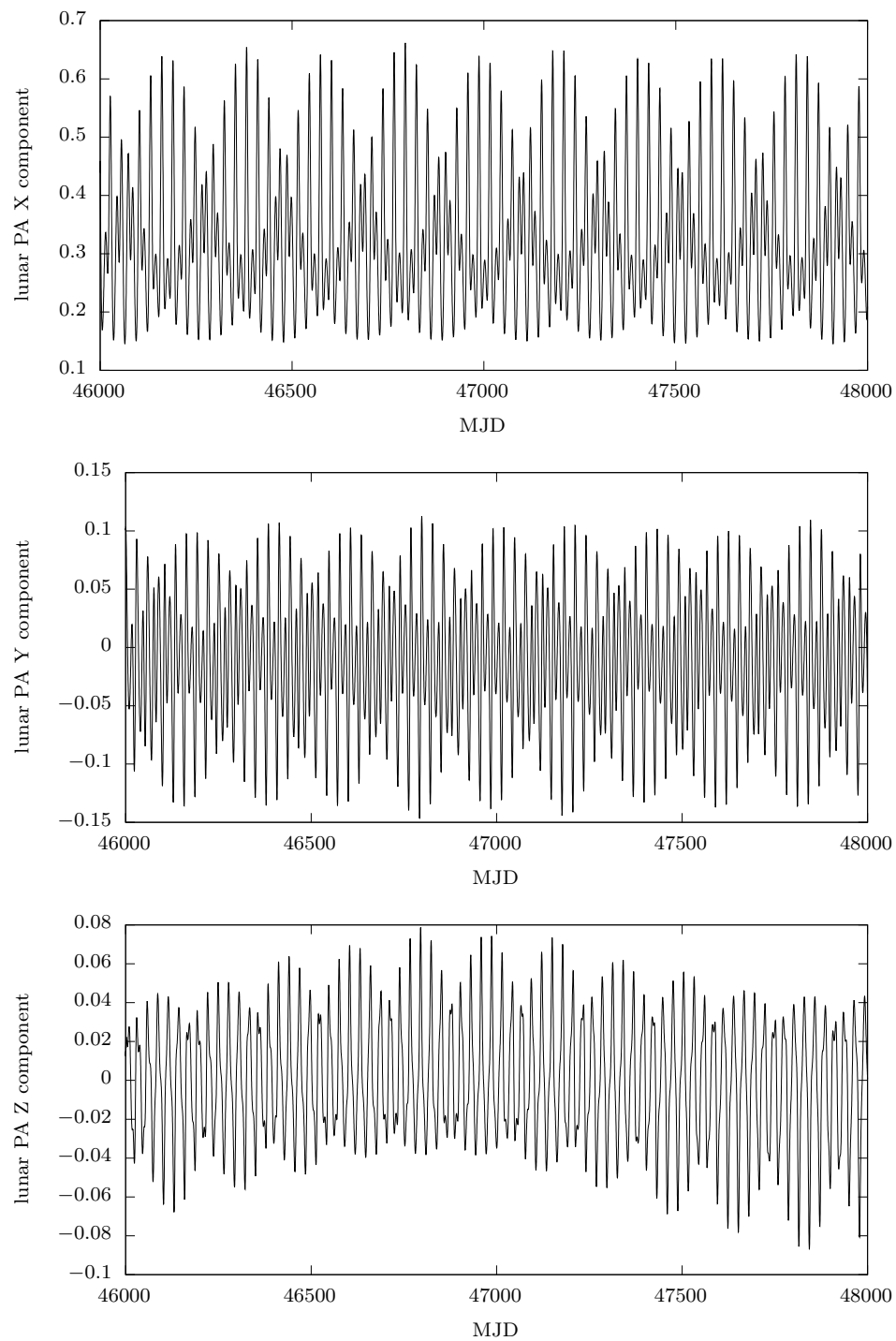
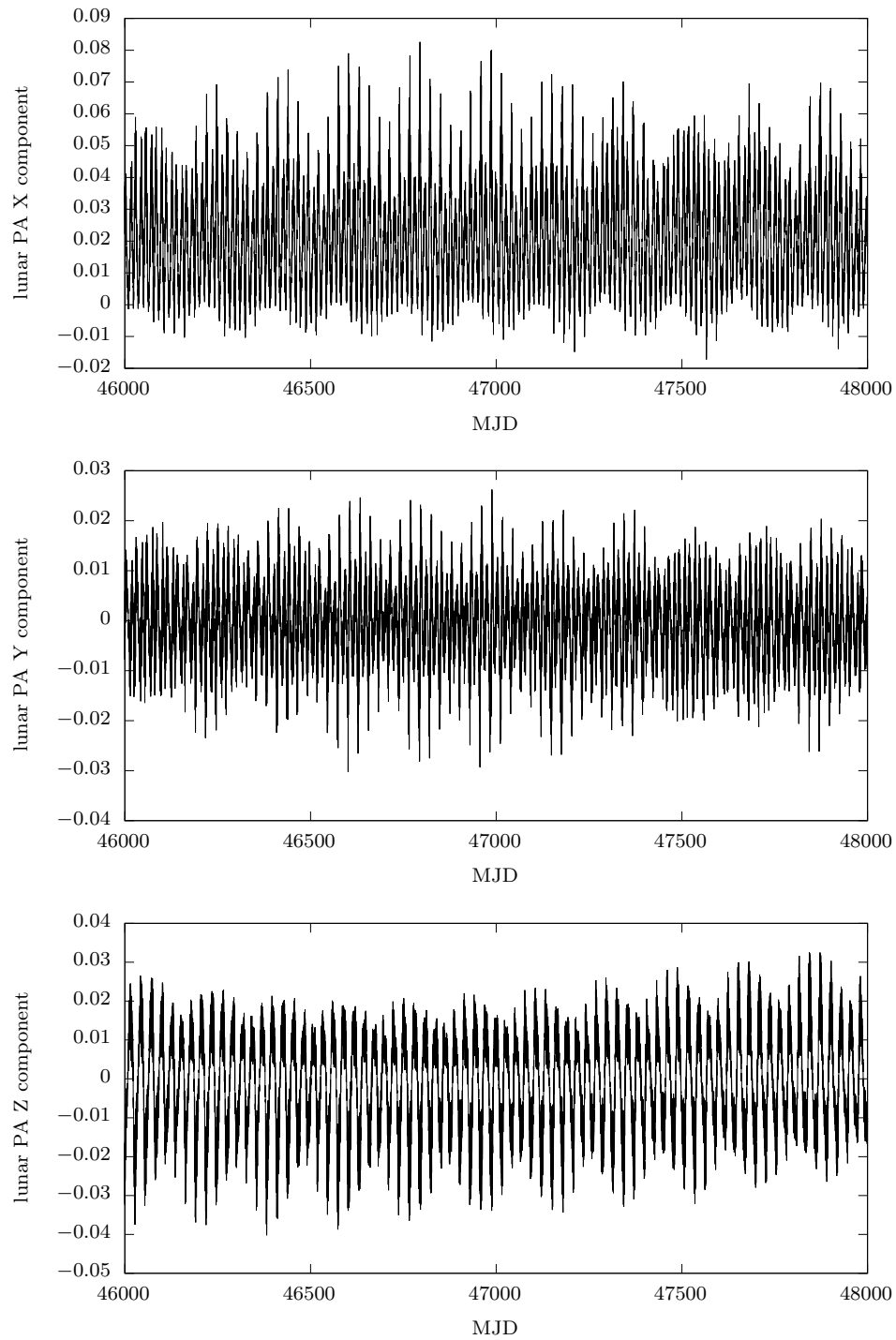
Fig. 3 Tidal acceleration according to the DE model, lunar frame, mm/day²

Fig. 4 DE tidal acceleration minus IERS acceleration on the same orbit, lunar frame, mm/day^2



7.3 Post-fit residuals of LLR observations

Post-fit statistics of observations for solutions I, II, and III are shown in Table 7. For each station, the number of utilized normal points is shown, followed by the number of points that have been automatically rejected, and then by the wrms deviation of $O - C$.

Station	Solution I			Solution II			Solution III		
	used	rej.	wrms	used	rej.	wrms	used	rej.	wrms
McDonald	3545	59	19.9	3545	59	20.1	3545	59	20.2
MLRS1	587	44	11.0	588	43	11.3	588	43	11.3
MLRS2	3210	443	3.5	3206	447	3.8	3207	446	3.8
Haleakala	748	22	5.4	750	20	5.8	750	20	5.8
Cerga (Ruby)	1109	79	17.2	1109	79	17.5	1109	79	17.5
Cerga (YAG)	8272	52	2.3	8271	53	2.4	8271	53	2.4
Cerga (MeO)	645	9	2.2	645	9	2.7	645	9	2.7
Apache	1546	27	1.4	1549	24	1.5	1539	34	1.5
Matera	64	19	3.8	63	20	3.3	63	20	3.3

Table 7 Post-fit statistics of solutions I-III. WRMS is one-way and given in cm.

The post-fit statistics of “e” counterparts of solutions I-III have been calculated and found to be nearly the same to as shown in Table 7, and are not listed here.

Plots of one-way $O - C$ of processed observations for selected stations are presented: Figure 5 for McDonald, MLRS1, and MLRS2, Figure 6 for CERGA, and Figure 7 for Apache Point.

7.4 Determined parameters

Parameters determined in solutions I-III, along with their formal uncertainties, are listed in Tables 8, 9, and 10. The initial parameters (except for stations' positions) are given at epoch JD 2446000.5.

Table 11 shows the extra eccentricity rates found in three “e” solutions.

7.5 Derived parameters

Secular tidal perturbation terms of the Earth-Moon system have been derived from Solution I using a table that converts the Love numbers and time delays (Williams and Boggs 2016), tidal acceleration $dn/dt \approx -25.901''/\text{cy}^2$, semimajor axis rate $da/dt \approx 38.204 \text{ mm/yr}$, and the eccentricity rate $de/dt \approx 13.4 \times 10^{-12}/\text{yr}$. The last figure is the modeled eccentricity rate, not including the found extra de/dt .

The lunar τ from Solution I indicates that $k_2/Q = 5.34 \times 10^{-4}$ or $Q = 45$ at a 1 month period, where Q is the tidal quality factor. The annual A_1 parameter gives $k_2/Q = 5.6 \times 10^{-4}$ or $Q = 45$ at a 1 year period.

The mean \bar{C}_{22} value can be calculated from determined β and γ :

$$\bar{C}_{22} = -\bar{C}_{20} \frac{\gamma(1 + \beta)}{2(2\beta - \gamma + \beta\gamma)} \frac{N_{20}}{N_{22}}. \quad (30)$$

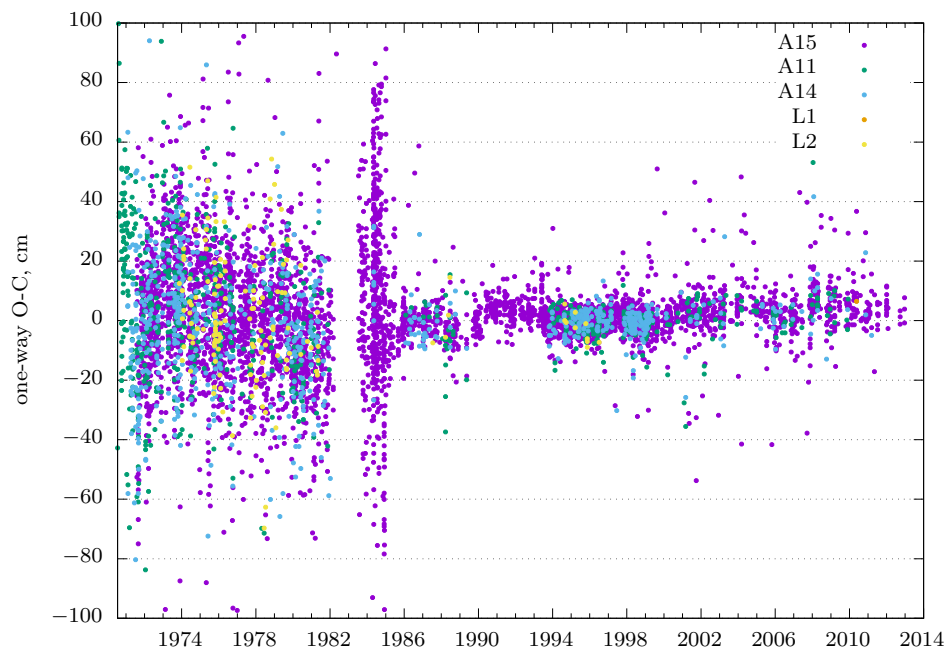
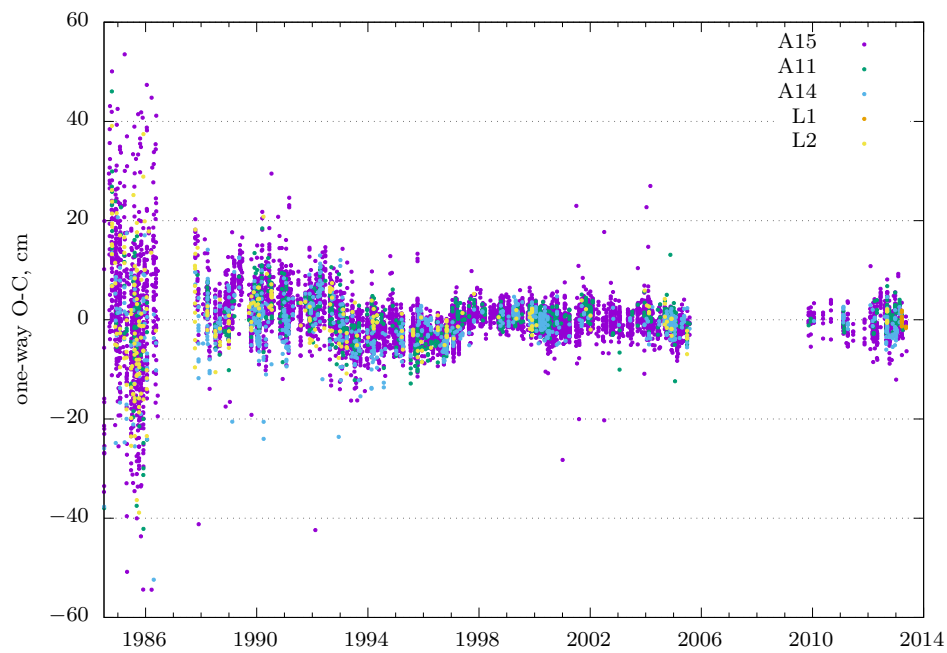
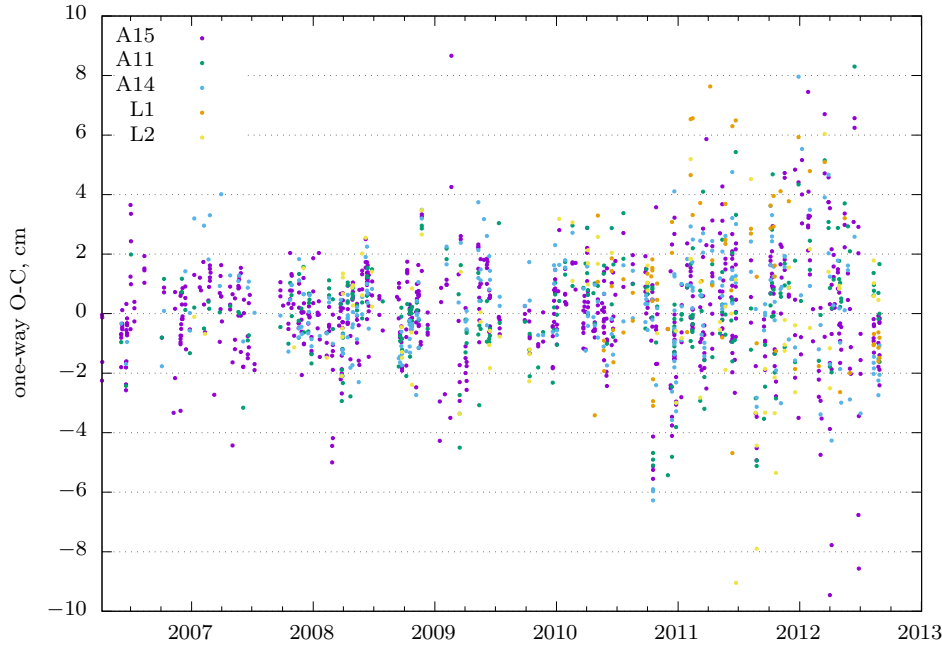
Fig. 5 Post-fit residuals for McDonald, MLRS1, and MLRS2 stations in Solution I**Fig. 6** Post-fit residuals for CERGA station in Solution I

Fig. 7 Post-fit residuals for Apache Point station in Solution I

Taking β and γ from solution I, one can find $\bar{C}_{22} = 0.346754 \times 10^{-4}$.

From the $\mu_E + \mu_M$ found in Solution I, and μ_E/μ_M fixed to 81.30056907, one can calculate $\mu_M = 4902.80008 \text{ km}^3/\text{s}^2$ and $\mu_E = 398600.4364 \text{ km}^3/\text{s}^2$.

8 Conclusion

The results of this work can be summarized as follows:

- Full implementation of DE430 lunar model was obtained and built into the EPM ephemeris software;
- The conventional model of Earth's gravitational potential has proven suitable for analyzing LLR observations;
- The IAU2000/2006 precession-nutation model along with the IERS C04 EOP series have proven suitable for analyzing LLR observations, with the only exception of IERS C04 before 1984 (JPL KEOF EOP series may be used instead);
- Secular tidal perturbation terms of the Earth-Moon system have been calculated: $dn/dt \approx -25.901''/\text{cy}^2$, $da/dt \approx 38.204 \text{ mm}/\text{yr}$, modeled $de/dt \approx 13.4 \times 10^{-12} \text{ /yr}$, extra $de/dt \approx 1.4 \times 10^{-12} \text{ /yr}$.
- Models of tidal station displacement from solid Earth tides and tropospheric delay, recommended in the IERS Conventions 2010, has proven suitable for analyzing LLR observations. The ocean loading model, though put to use, has not been checked thoroughly; atmospheric loading and ocean pole tide loading were not implemented;

Parm.	Solution I value	Solution II value	Solution III value	units
$r_{EM,x}$	-137136474.05 ± 0.05	-137136473.33 ± 0.05	-137136473.43 ± 0.06	m
$r_{EM,y}$	-311514604.01 ± 0.05	-311514604.25 ± 0.05	-311514604.22 ± 0.06	m
$r_{EM,z}$	-141738600.43 ± 0.04	-141738600.26 ± 0.05	-141738600.17 ± 0.05	m
$\dot{r}_{EM,x}$	962372276.11 ± 0.13	962372276.35 ± 0.14	962372276.14 ± 0.14	$\mu\text{m}/\text{sec}$
$\dot{r}_{EM,y}$	-375608190.19 ± 0.14	-375608188.59 ± 0.15	-375608188.88 ± 0.14	$\mu\text{m}/\text{sec}$
$\dot{r}_{EM,z}$	-268439311.42 ± 0.06	-268439310.06 ± 0.06	-268439310.14 ± 0.07	$\mu\text{m}/\text{sec}$
$\omega_{c,x}$	$(-890 \pm 4) \cdot 10^{-6}$	$(-920 \pm 4) \cdot 10^{-6}$	$(-932 \pm 4) \cdot 10^{-6}$	rad/day
$\omega_{c,y}$	$(-6453 \pm 8) \cdot 10^{-6}$	$(-6496 \pm 8) \cdot 10^{-6}$	$(-6484 \pm 8) \cdot 10^{-6}$	rad/day
$\omega_{c,z}$	$(229.63 \pm 0.05) \cdot 10^{-3}$	$(230.32 \pm 0.03) \cdot 10^{-3}$	$(230.22 \pm 0.02) \cdot 10^{-3}$	rad/day
ϕ	$(-5823800 \pm 2) \cdot 10^{-8}$	$(-5823802 \pm 2) \cdot 10^{-8}$	$(-5823821 \pm 2) \cdot 10^{-8}$	rad
θ	$(39511625 \pm 1) \cdot 10^{-8}$	$(39511623 \pm 1) \cdot 10^{-8}$	$(39511618 \pm 1) \cdot 10^{-8}$	rad
ψ	$(113574562 \pm 3) \cdot 10^{-8}$	$(113574584 \pm 3) \cdot 10^{-8}$	$(113574591 \pm 3) \cdot 10^{-8}$	rad
$\dot{\phi}$	-74.537 ± 0.001	-74.541 ± 0.001	-74.543 ± 0.001	"/day
$\dot{\theta}$	-37.0255 ± 0.0003	-37.0257 ± 0.0004	-37.0227 ± 0.0004	"/day
$\dot{\psi}$	47501.853 ± 0.001	47501.859 ± 0.001	47501.862 ± 0.001	"/day
$\mu_E + \mu_M$	403503.2365 ± 0.0002	403503.2360 ± 0.0002	403503.2358 ± 0.0002	km^3/s^2
β	$(631023.1 \pm 0.5) \cdot 10^{-9}$	$(631024.5 \pm 0.5) \cdot 10^{-9}$	$(631024.9 \pm 0.5) \cdot 10^{-9}$	1
γ	$(227733.3 \pm 0.7) \cdot 10^{-9}$	$(227736.0 \pm 0.7) \cdot 10^{-9}$	$(227736.3 \pm 0.7) \cdot 10^{-9}$	1
τ	0.096 ± 0.001	0.079 ± 0.001	0.075 ± 0.001	day
τ_{1R}	0.00787 ± 0.00005	N/A	N/A	day
τ_{2R}	0.002855 ± 0.000004	N/A	N/A	day
f_c	$(0.247 \pm 0.004) \cdot 10^{-3}$	$(0.249 \pm 0.004) \cdot 10^{-3}$	$(0.245 \pm 0.004) \cdot 10^{-3}$	1
k_v/C_T	$(16.3 \pm 0.2) \cdot 10^{-9}$	$(18.6 \pm 0.2) \cdot 10^{-9}$	$(19.4 \pm 0.2) \cdot 10^{-9}$	day^{-1}
h_2	0.043 ± 0.001	0.041 ± 0.001	0.041 ± 0.001	1
A_1	4.6 ± 0.2	4.3 ± 0.2	4.4 ± 0.2	mas
A_2	1.4 ± 0.2	0.7 ± 0.2	0.4 ± 0.2	mas
A_3	-7.4 ± 0.5	-10.3 ± 0.5	-12.0 ± 0.5	mas
\hat{C}_{32}	$(14184.3 \pm 0.3) \cdot 10^{-9}$	$(14185.5 \pm 0.4) \cdot 10^{-9}$	$(14184.9 \pm 0.3) \cdot 10^{-9}$	1
\hat{S}_{32}	$(4931.8 \pm 0.6) \cdot 10^{-9}$	$(4937.4 \pm 0.7) \cdot 10^{-9}$	$(4896.3 \pm 0.6) \cdot 10^{-9}$	1
\hat{C}_{33}	$(11975 \pm 11) \cdot 10^{-9}$	$(11912 \pm 11) \cdot 10^{-9}$	$(11913 \pm 11) \cdot 10^{-9}$	1
A11 x	1591966.90 ± 0.06	1591966.80 ± 0.06	1591966.72 ± 0.06	m
A11 y	690699.56 ± 0.04	690699.32 ± 0.04	690699.47 ± 0.04	m
A11 z	21003.73 ± 0.02	21003.76 ± 0.02	21003.78 ± 0.02	m
A14 x	1652689.86 ± 0.06	1652689.63 ± 0.07	1652689.65 ± 0.06	m
A14 y	-520997.46 ± 0.04	-520997.78 ± 0.05	-520997.58 ± 0.04	m
A14 z	-109730.52 ± 0.02	-109730.47 ± 0.02	-109730.52 ± 0.02	m
A15 x	1554678.60 ± 0.07	1554678.41 ± 0.07	1554678.39 ± 0.06	m
A15 y	98095.64 ± 0.04	98095.32 ± 0.04	98095.26 ± 0.04	m
A15 z	765005.14 ± 0.03	765005.19 ± 0.03	765005.17 ± 0.04	m
L1 x	1114292.57 ± 0.06	1114292.29 ± 0.06	1114292.35 ± 0.06	m
L1 y	-781298.47 ± 0.04	-781298.82 ± 0.04	-781298.99 ± 0.04	m
L1 z	1076058.49 ± 0.03	1076058.38 ± 0.04	1076058.34 ± 0.06	m
L2 x	1339363.66 ± 0.06	1339363.56 ± 0.06	1339363.48 ± 0.06	m
L2 y	801872.04 ± 0.04	801871.80 ± 0.04	801871.73 ± 0.04	m
L2 z	756358.60 ± 0.03	756358.62 ± 0.03	756358.65 ± 0.03	m

Table 8 Determined parameters and their formal uncertainties, part 1

- In addition to the DE430 model of tidal acceleration of the orbit of the Moon, the ‘‘IERS 2010’’ model of tidal variations of the geopotential has been implemented. It has been found that the IERS model fits slightly worse to LLR observations, though that was not unexpected given two fewer solution parameters. It has been found that lunar τ and extra de/dt are very sensitive to the tidal model used; in particular, the extra eccentricity rate falls from 1.4×10^{-12} with the DE model to -1.3×10^{-12} with the IERS model;

Parameter	Solution I value	Solution II value	Solution III value	units
McD λ	255.978002(5 ± 1)	255.978002(3 ± 1)	255.978002(3 ± 1)	°
McD $r \cos \phi$	5492414.46 ± 0.03	5492414.45 ± 0.03	5492414.45 ± 0.03	m
McD $r \sin \phi$	3235697.50 ± 0.02	3235697.50 ± 0.02	3235697.51 ± 0.02	m
MLRS1 λ	255.984120(8 ± 1)	255.984120(9 ± 1)	255.984120(9 ± 1)	°
MLRS1 $r \cos \phi$	5492037.71 ± 0.03	5492037.67 ± 0.04	5492037.67 ± 0.04	m
MLRS1 $r \sin \phi$	3236146.76 ± 0.02	3236146.75 ± 0.02	3236146.75 ± 0.02	m
MLRS2 λ	255.9848036(6 ± 3)	255.9848036(5 ± 3)	255.9848036(5 ± 3)	°
MLRS2 $r \cos \phi$	5491888.44 ± 0.01	5491888.44 ± 0.01	5491888.43 ± 0.01	m
MLRS2 $r \sin \phi$	3236481.64 ± 0.01	3236481.62 ± 0.01	3236481.63 ± 0.01	m
Apache λ	254.17957680(8 ± 7)	254.17957679(3 ± 8)	254.17957679(2 ± 8)	°
Apache $r \cos \phi$	5370045.373 ± 0.002	5370045.376 ± 0.002	5370045.378 ± 0.002	m
Apache $r \sin \phi$	3435012.897 ± 0.002	3435012.913 ± 0.002	3435012.910 ± 0.002	m
CERGA λ	6.9215727(8 ± 1)	6.9215727(5 ± 1)	6.9215727(5 ± 1)	°
CERGA $r \cos \phi$	4615328.454 ± 0.002	4615328.450 ± 0.002	4615328.450 ± 0.002	m
CERGA $r \sin \phi$	4389355.103 ± 0.003	4389355.106 ± 0.003	4389355.107 ± 0.003	m
Haleakala λ	203.7440954(3 ± 3)	203.7440955(6 ± 3)	203.7440955(8 ± 3)	°
Haleakala $r \cos \phi$	5971474.51 ± 0.01	5971474.53 ± 0.01	5971474.53 ± 0.01	m
Haleakala $r \sin \phi$	2242188.41 ± 0.01	2242188.43 ± 0.01	2242188.44 ± 0.01	m
Matera λ	16.704613(5 ± 7)	16.704613(3 ± 2)	16.704613(3 ± 2)	°
Matera $r \cos \phi$	4846504.3 ± 0.2	4846504.25 ± 0.04	4846504.24 ± 0.04	m
Matera $r \sin \phi$	4133249.58 ± 0.05	4133249.59 ± 0.01	4133249.58 ± 0.02	m
McD $\dot{\lambda}$	-0.53 ± 0.01	-0.56 ± 0.01	-0.56 ± 0.01	mas/yr
McD ($r \cos \phi$) $\dot{\phi}$	3.5 ± 0.2	2.8 ± 0.2	2.9 ± 0.2	mm/yr
McD ($r \sin \phi$) $\dot{\phi}$	3.5 ± 0.5	4.2 ± 0.5	3.7 ± 0.5	mm/yr
CERGA $\dot{\lambda}$	0.915 ± 0.007	0.914 ± 0.007	0.913 ± 0.008	mas/yr
CERGA ($r \cos \phi$) $\dot{\phi}$	-15.7 ± 0.2	-16.5 ± 0.2	-16.5 ± 0.2	mm/yr
CERGA ($r \sin \phi$) $\dot{\phi}$	14.3 ± 0.4	13.9 ± 0.4	13.8 ± 0.4	mm/yr

Table 9 Determined parameters and their formal uncertainties, part 2: stations

- Non-zero mean value of lunar $\bar{S}_{21}^{(0)}$, taken from GRAIL, does not make any significant difference in postfit results and does not affect much the determined parameters of lunar inner structure; similar tests (not shown in the results) were done for $\bar{C}_{21}^{(0)}$ and $\bar{S}_{22}^{(0)}$, with similar outcomes.
- The strong detection of k_v/C_T demonstrates that the Moon has a fluid core.
- The lunar τ indicates substantial tidal dissipation with $Q = 45$ at a 1-month period and the annual A_1 parameter shows similarly strong dissipation with $Q = 45$ at a 1-year period.
- Determined \bar{C}_{32} differs from the GL660b value (1.41715×10^{-5}) by $< 0.1\%$; derived \bar{C}_{22} is also very close to GL660b value (0.346737×10^{-4});
- The determined \bar{S}_{32} value differs from the GL660b value (4.8780×10^{-6}) by 0.4–1.2%, depending on the solution; the determined \bar{C}_{33} value differs by some 3% from the GL660b value (1.2275×10^{-5}).

More research is needed to find the cause of the difference between the values of \bar{S}_{32} and \bar{C}_{33} determined from LLR and GRAIL, and the cause of the misalignment of the lunar PA frame in the model with the GRAIL's frame. A separate direction of research is the influence of the IERS tidal model on the eccentricity rate.

Acknowledgements D. Pavlov would like to thank Elena Pitjeva, Eleonora Yagudina, Sergey Kurubov, Vladimir Skripnichenko, and numerous other colleagues from the IAA RAS for helpful comments and advice throughout this work; and Matthew Flatt from the University of Utah for his help in programming on the Racket platform.

Parameter	Solution I value	Solution II value	Solution III value	units
Bias 1 (APOLLO)	6.4 ± 1.1	7.7 ± 1.2	8.2 ± 1.2	cm
Bias 2 (APOLLO)	10.9 ± 1.1	12.6 ± 1.2	13.1 ± 1.2	cm
Bias 3 (APOLLO)	3.3 ± 1.1	5.0 ± 1.2	5.3 ± 1.2	cm
Bias 4 (APOLLO)	12.1 ± 1.2	12.6 ± 1.3	13.1 ± 1.3	cm
Bias 5 (APOLLO)	-1.7 ± 1.1	-1.1 ± 1.2	-0.4 ± 1.2	cm
Bias 6 (CERGA)	23.1 ± 1.9	30.8 ± 2.1	30.6 ± 2.0	cm
Bias 7 (CERGA)	4.1 ± 1.1	5.2 ± 1.2	5.2 ± 1.2	cm
Bias 8 (CERGA)	-11.7 ± 1.5	-7.3 ± 1.6	-7.2 ± 1.6	cm
Bias 9 (CERGA)	-13.5 ± 1.2	-11.5 ± 1.2	-11.7 ± 1.2	cm
Bias 10 (CERGA)	6.0 ± 1.7	11.8 ± 1.8	11.2 ± 1.8	cm
Bias 11 (CERGA)	4.8 ± 2.1	11.7 ± 2.2	11.7 ± 2.2	cm
Bias 12 (CERGA)	-4.0 ± 1.2	-6.0 ± 1.3	-5.5 ± 1.3	cm
Bias 13 (Haleakala)	-0.6 ± 1.7	1.9 ± 1.8	2.1 ± 1.7	cm
Bias 14 (Haleakala)	8.3 ± 1.9	14.3 ± 0.2	14.6 ± 2.0	cm
Bias 15 (Haleakala)	-11.7 ± 1.8	-9.1 ± 1.9	-9.0 ± 1.9	cm
Bias 16 (Haleakala)	3.0 ± 2.4	2.9 ± 2.5	3.3 ± 2.5	cm
Bias 17 (Haleakala)	38.3 ± 4.0	37.7 ± 4.3	37.8 ± 4.2	cm
Bias 18 (Haleakala)	40.5 ± 3.2	47.1 ± 3.4	48.2 ± 3.3	cm
Bias 19 (Haleakala)	24.3 ± 1.9	27.4 ± 2.1	27.5 ± 2.0	cm
Bias 20 (Haleakala)	-9.5 ± 1.8	-3.8 ± 1.9	-3.4 ± 1.9	cm
Bias 21 (McDonald)	42.0 ± 4.9	42.3 ± 5.2	42.6 ± 5.2	cm
Bias 22 (McDonald)	28.3 ± 5.3	29.5 ± 5.7	30.0 ± 5.7	cm
Bias 23 (McDonald)	-52.8 ± 18.3	-52.5 ± 19.6	-53.2 ± 19.4	cm
Bias 24 (McDonald)	160.1 ± 6.8	162.6 ± 7.3	163.8 ± 7.3	cm
Bias 25 (McDonald)	22.2 ± 6.3	20.7 ± 6.8	22.0 ± 6.7	cm
Bias 26 (McDonald)	-22.4 ± 14.9	-11.1 ± 16.0	-11.0 ± 15.8	cm
Bias 27 (Matera)	23.6 ± 35.8	5.1 ± 7.6	3.7 ± 7.5	cm
Bias 28 (MLRS1)	6.0 ± 6.2	1.8 ± 6.6	2.1 ± 6.5	cm

Table 10 Determined parameters and their formal uncertainties, part 3: biases (two-way)

Solution	extra de/dt , yr^{-1}	1σ , yr^{-1}
Ie	1.4×10^{-12}	0.2×10^{-12}
IIe	-1.3×10^{-12}	0.2×10^{-12}
IIIe	-1.4×10^{-12}	0.2×10^{-12}

Table 11 Extra eccentricity rate and its formal uncertainty in obtained solutions

This work would not have been possible without the effort of personnel at observatories doing lunar laser ranging: Apache Point (Murphy et al. 2012; Murphy 2013), McDonald Laser Ranging Station (Shelus 1985), Observatoire de la Côte d’Azur (Samain et al. 1998), Giuseppe Bianco at Matera Laser Ranging Observatory, and Lunar Ranging Experiment (LURE) at the Haleakala observatory in the past. The POLAC website was of great help, where Christophe Barache, Sébastien Bouquillon, Teddy Carlucci, and Gerard Francou carefully collected LLR observations from different sources.

An anonymous reviewer provided a lot of comments and suggestions that allowed to improve the article substantially.

A portion of the research described in this paper was carried out at the Jet Propulsion Laboratory of the California Institute of Technology, under a contract with the National Aeronautics and Space Administration. Government sponsorship acknowledged.

References

- Avdyushev, V.: Gauss–Everhart Integrator (in Russian). *Computational Technologies (Vychislitelnye Tekhnologii)* **15**, 31–46 (2010)
- Bizouard, C., Gambis, D.: The Combined Solution C04 for Earth Orientation Parameters Consistent with International Terrestrial Reference Frame 2005. In: Drewes, H. (ed.) *Geodetic Reference Frames: IAG Symposium Munich, Germany, 9-14 October 2006*, pp. 265–270. Springer Berlin Heidelberg (2009)
- Bizouard, C., Gambis, D.: The combined solution C04 for Earth Orientation Parameters consistent with International Terrestrial Reference Frame 2008. *IERS notice* (2011). <http://hpiers.obspm.fr/iers/eop/eopc04/C04.guide.pdf>
- Chapront-Touzé, M., Chapront, J.: ELP 2000-85 — A semi-analytical lunar ephemeris adequate for historical times. *A&A* **190**(1-2), 342–352 (1998)
- Cunningham, L.E.: On the computation of the spherical harmonic terms needed during the numerical integration of the orbital motion of an artificial satellite. *Celestial Mechanics and Dynamical Astronomy* **2**(2), 207–216 (1970)
- Ferland, R., Piraszewski, M.: The IGS-combined station coordinates, earth rotation parameters and apparent geocenter. *Journal of Geodesy* **83**(3), 385–392 (2009)
- Fienga, A., Laskar, J., Gastineau, M., Verma, A.: INPOP new release: INPOP13c. Tech. rep., Observatoire de Paris (2013). URL <http://www.imcce.fr/fr/presentation/equipement/ASD/inpop/inpop13c.pdf>
- Findler, R., Clements, J., Flanagan, C., Flatt, M., Krishnamurthi, S., Steckler, P., Felleisen, M.: DrScheme: A programming environment for Scheme. *Journal of Functional Programming* **12**(2), 159–182 (2002)
- Finkelstein, A.M., Ipatov, A.V., Skurikhina, E.A., Surkis, I.F., Smolentsev, S.G., Fedotov, L.V.: Geodynamic observations on the quasar VLBI network in 2009–2011. *Astronomy Letters* **38**(6), 394–398 (2012)
- Flatt, M., PLT: Reference: Racket. Tech. Rep. PLT-TR-2010-1, PLT Design Inc. (2010). <http://racket-lang.org/tr1/>
- Folkner, W., Williams, J., Boggs, D., Park, R., Kuchynka, P.: The Planetary and Lunar Ephemerides DE430 and DE431. IPN Progress Report 42-196, NASA JPL (2014)
- Hohenkerk, C.: SOFA and the algorithms for transformations between time scales and between reference systems. In: Schuh, H., Bhm, S., Nilsson, T., Capitaine, N. (eds.) *Proceedings of the Journées 2011 “Systèmes de référence spatio-temporels”*, pp. 21–24. Vienna University of Technology (2012)
- Konopliv, A.S., Park, R.S., Yuan, D.N., Asmar, S.W., Watkins, M.M., Williams, J.G., Fahnestock, E., Kruizinga, G., Paik, M., Strelakov, D., Harvey, N., Smith, D.E., Zuber, M.T.: The JPL lunar gravity field to spherical harmonic degree 660 from the GRAIL Primary Mission. *Journal of Geophysical Research: Planets* **118**(7), 1415–1434 (2013)
- Kopeikin, S.M.: Theory of Relativity in Observational Radio Astronomy. *Sov. Astron.* **34**(1), 5–9 (1990)
- Krasinsky, G., Prokhorenko, S., Yagudina, E.: New version of EPM-ERA lunar theory. In: Capitaine, N. (ed.) *Proceedings of the Journées 2010 “Systèmes de référence spatio-temporels”*, pp. 61–64. Observatoire de Paris (2011)
- Krasinsky, G., Vasilyev, M.: ERA-7. Knowledge Base and Programming System for Dynamical Astronomy: Manual. Institute of Applied Astronomy RAS (2006)

- Krasinsky, G.A.: Selenodynamical parameters from analysis of LLR observations of 1970-2001. *Communications of the IAA RAS* **148**, 1–27 (2002)
- Krasinsky, G.A., Novikov, F.A., Scripnichenko, V.I.: Problem Oriented Language for Ephemeris Astronomy and its Realisation in the System ERA. *Celestial Mechanics* **45**(1), 219–229 (1988)
- Krasinsky, G.A., Vasilyev, M.V.: Era: Knowledge Base for Ephemeris and Dynamical Astronomy. In: Wyrzyszcak, I.M., Lieske, J.H., Feldman, R.A. (eds.) *Dynamics and Astrometry of Natural and Artificial Celestial Bodies: Proceedings of IAU Colloquium 165 Poznań, Poland July 1 – 5, 1996*, pp. 239–244. Springer Netherlands, Dordrecht (1997)
- Manche, H., Bouquillon, S., Fienga, A., Laskar, J., Francou, G.: Towards INPOP07, adjustments to LLR data. In: Capitaine, N. (ed.) *Proceedings of the Journées 2007 “Systèmes de référence spatio-temporels”*, pp. 70–73. Observatoire de Paris (2008)
- Manche, H., Fienga, A., Laskar, J., Bouquillon, S., Francou, G., Gastineau, M.: LLR residuals of INPOP10a and constraints on post-newtonian parameters. In: Schuh, H., Bhm, S., Nilsson, T., Capitaine, N. (eds.) *Proceedings of the Journées 2011 “Systèmes de référence spatio-temporels”*, pp. 65–68. Vienna University of Technology (2012)
- Mathews, P.M., Dehant, V., Gipson, J.M.: Tidal station displacements. *Journal of Geophysical Research: Solid Earth* **102**(B9), 20,469–20,477 (1997)
- Mendes, V.B., Pavlis, E.C.: High-accuracy zenith delay prediction at optical wavelengths. *Geophysical Research Letters* **31**(14) (2004)
- Mendes, V.B., Prates, G., Pavlis, E.C., Pavlis, D.E., Langley, R.B.: Improved mapping functions for atmospheric refraction correction in SLR. *Geophysical Research Letters* **29**(10), 53–1–53–4 (2002)
- Murphy, T.: Lunar laser ranging: the millimeter challenge. *Rep. Prog. Phys.* **76**, 076,901 (2013)
- Murphy, T., Adelberger, E., Battat, J., Hoyle, C., Johnson, N., McMillan, R., Stubbs, C., Swanson, H.: APOLLO: millimeter lunar laser ranging. *Class. Quantum Grav.* **29**, 184,005 (2012)
- Newhall, X., Williams, J.G., Dickey, J.O.: Earth rotation (UTO-UTC) from lunar laser ranging. In: *IERS Technical Note No. 5*, pp. 41–45 (1990)
- Pavlov, D., Skripnichenko, V.: Rework of the ERA software system: ERA-8. In: Malkin, Z., Capitaine, N. (eds.) *Proceedings of the Journées 2014 “Systèmes de référence spatio-temporels”*, pp. 243–246. Pulkovo Observatory (2015)
- Petit, G., Luzum, B.: *IERS Conventions 2010 (IERS Technical Note 36)*. Verlag des Bundesamts für Kartographie und Geodäsie, Frankfurt am Main (2010)
- Pitjeva, E.: Updated IAA RAS planetary ephemerides-EPM2011 and their use in scientific research. *Sol. Syst. Res.* **47**(5), 386–402 (2013)
- Pitjeva, E., Pitjev, N.: Development of planetary ephemerides EPM and their applications. *Cel. Mech. and Dyn. Astron.* **119**(3–4), 237–256 (2014)
- Ratcliff, J., Gross, R.: *Combinations of Earth Orientation Measurements: SPACE2014, COMB2014, and POLE2014*. Jpl publication 15-8, NASA (2015)
- Samain, E., Mangin, J., Veillet, C., Torre, J.M., Fridelance, P., Chabaudie, J., Féraudy, D., Glentzlin, M., Pham Van, J., Furia, M., Journet, A., Vigouroux, G.: Millimetric lunar laser ranging at OCA (Observatoire de la Côte d’Azur). *Astron. Astrophys. Suppl. Ser.* **130**, 235–244 (1998)

- Shelus, P.J.: MLRS: a lunar/artificial satellite laser ranging facility at the McDonald Observatory. *IEEE Trans. on Geosci. and Rem. Sens.* **GE-234**, 385–390 (1985)
- Standish, E., Newhall, X., Williams, J., Yeomans, D.: *Orbital Ephemerides of the Sun, Moon, and Planets*. In: Seidelmann, P.K. (ed.) *Explanatory Supplement to the Astronomical Almanac*. University Science Books (1992)
- Vasilyev, M., Yagudina, E.: Russian lunar ephemeris EPM-ERA 2012. *Sol. Syst. Res.* **48**(2), 158–165 (2014)
- Williams, J., Boggs, D.: Tides on the Moon: Theory and determination of dissipation. *J. Geophys. Res.* **120**, 689–724 (2015)
- Williams, J., Boggs, D.: Secular tidal changes in lunar orbit and Earth rotation. Submitted to *Celest. Mech. Dyn. Astron.* (2016)
- Williams, J.G., Boggs, D.H., Folkner, W.M.: DE430 Lunar Orbit, Physical Librations, and Surface Coordinates. Jet Propulsion Laboratory Interoffice Memorandum 335-JW,DB,WF-20130722-016, California Institute of Technology (2013)
- Williams, J.G., Boggs, D.H., Yoder, C.F., Ratcliff, J.T., Dickey, J.O.: Lunar rotational dissipation in solid body and molten core. *Journal of Geophysical Research: Planets* **106**(E11), 27,933–27,968 (2001)
- Williams, J.G., Konopliv, A.S., Boggs, D.H., Park, R.S., Yuan, D.N., Lemoine, F.G., Goossens, S., Mazarico, E., Nimmo, F., Weber, R.C., Asmar, S.W., Melosh, H.J., Neumann, G.A., Phillips, R.J., Smith, D.E., Solomon, S.C., Watkins, M.M., Wiczorek, M.A., Andrews-Hanna, J.C., Head, J.W., Kiefer, W.S., Matsuyama, I., McGovern, P.J., Taylor, G.J., Zuber, M.T.: Lunar interior properties from the GRAIL mission. *Journal of Geophysical Research: Planets* **119**(7), 1546–1578 (2014)